FRONTIERS OF PHYSICS

TOPICAL REVIEW
Volume 18 / Issue 5 / 53604 / 2023

Defect repairing in two-dimensional transition metal dichalcogenides

Shiyan Zeng, Fang Li, Chao Tan, Lei Yang, Zegao Wang†

College of Materials Science and Engineering, Sichuan University, Chengdu 610065, China
Corresponding author. E-mail: †zegao@scu.edu.cn
Received February 13, 2023; accepted March 30, 2023

ABSTRACT

Atomically thin two-dimensional (2D) transition metal dichalcogenides (TMDCs) have stimulated enormous research interest due to rich phase structure, high theoretical carrier mobility and layer-dependent bandgap. In view of the close correlation between defects and properties in 2D TMDCs, more attentions have been paid on the defect engineering in recent years, however the mechanism is still unclear. Herein, we review the critical progress of defect engineering and provide an extensive way to modulate the properties depressed by defects. To insight into the defect engineering, we firstly introduce two common kinds of defects during the growth progress of TMDCs and the possible distribution of energy levels those defects could induce. Then, various methods to improve point defects and grain boundaries during the period of growth are discussed intensively, with the assistance of which more large-area TMDCs films can be obtained. Considering the defects in TMDCs are inevitable regardless of concentration, we also highlight strategies to heal the defects after growth. Through dry methods or wet methods, the chalcogen vacancies can be repaired and thus, the performance of electronic device would be significantly enhanced. Finally, we propose the challenges and prospective for defect engineering in 2D TMDCs materials to support the optimization of device and lead them to wide applied fields.

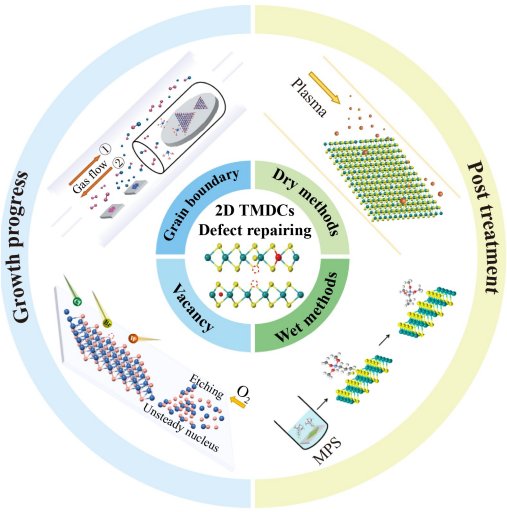

Keywords defect, repairing, two-dimensional transition metal, dichalcogenides

Contents

1 Introduction 2
2 Defect types 3
2.1 Point defect 3
2.2 Grain boundary 3
3 Improve the quality during the growth 5
3.1 Vacancy 5
3.2 Grain boundary 6
4 Improve the quality by post-treatment 7
4.1 Sulfur vacancy 7
4.1.1 Post-treatment by dry method 7
4.1.2 Post-treatment by wet method 8
4.2 Selenium vacancy repair 10
4.2.1 Post-treatment by dry method 10
4.2.2 Post-treatment by wet method 10
5 Conclusion and outlook 11
5.1 Revealing defect repairing mechanism 12
5.2 Optimizing repairing process design 12

Special Topic: Surface and Interface of Two-dimensional Materials (Eds.: Lijun Zhang, Dongchen Qi, Ming Yang & Kai Zhang).

Higher Education Press

https://doi.org/10.1007/s11467-023-1290-6

Acknowledgements 12
References 12

1 Introduction

Two-dimensional (2D) materials have inspired a new research wave attempting to extend Moore's Law and realize future electronic device miniaturization in the past decade since the discovery and rapid development of grapheme [1–4]. Numerous researches have revealed that graphene's special zero-bandgap bring about low on/off ratio, which is unsatisfactory for applications in logic electronic and optoelectronic devices [2, 5]. Since then, a variety of graphene analogs with the same atomically-thin layered structure have been extensively investigated for their abundant fantastic properties [5–8]. Transition metal dichalcogenides (TMDCs), which refer to a unique class of 2D materials with a sandwich structure where one layer of transition metal atoms is between two layers of chalcogen atoms [9], have displayed adjustable band gaps [10], high on/off ratio [11] and extraordinary photoresponsivity [12]. In addition, rich structural phases corresponding to different coordination and stacking order of metal and chalcogen atoms endow TMDCs a wealth of electronic and optoelectronic properties [13–17]. All of these outstanding features have put TMDCs in the position of promising candidates for next-generation nanoelectronics [18, 19]. However, the actual performance of devices based on 2D TMDCs is far from the theoretical prediction by reason of the inevitable intrinsic defects in materials [20–22]. Heretofore, more significant efforts have been devoted to the defect engineering to improve the quality of TMDCs availably and remarkably.

In contrast to the bulk state, the nature of 2D TMDCs seems easier to be changed by different kinds of defects including vacancy, adatom, substitution and grain boundary due to the atomically thin structure [5]. Specifically, the optical, electronic and optoelectronic properties of ultrathin TMDCs are all under the defect influence prominently [23–25]. For instance, the sulfur vacancies in molybdenum disulfide (MoS_2) could act as electron donors and increase the electron concentration to bring in n-type doping, so that the extra electrons tend to make trions negative and lower excitonic photoluminescence (PL) intensity [26–29]. On the other hand, the defects would have a great impact on the transport of conduction electron, which could serve as scattering centers and increase the probability of carrier scattering, sequentially leading to the low carrier mobility [26]. To further study those intricate defects and precisely lessen unfavorable defects, it is necessary to utilize the advanced modern technologies of characterization to detect the defects existed in TMDCs at the atomic level. Multiple ways including scanning tunneling microscopy (STM) [30], transmission electron microscopy (TEM) [31] and scanning transmission electron microscope (STEM) [32] could confirm the defect type and number, which can give a more accurate analysis on different kinds of defects. At present, plenty of approaches specific to the defect repairing have been demonstrated by experiments to improve the crystalline quality, such as regulating the growth parameters to increase the concentration of chalcogens in TMDCs [33], choosing appropriate substrates [34], sources [35] and additives [36], post annealing treatment in a certain temperature and flow rate [37]. Moreover, extra protection layers (i.e., grapheme [38] and h-BN [39]), are also proved to prevent the formation of defects during the subsequent process of characterization and using. Although the investigations are extensive and the repair methods for defects are diverse, there seems to be a lack of systematic summary on the repairing techniques classified according to the typical defect types for the moment.

In this manuscript, we have reviewed the latest progress of defect engineering in 2D TMDCs triggered by the growth process and provide a coherent research idea for future studies on intrinsic defects introduced by growth. The scope of this review is shown in Fig. 1. Firstly, we emphasize two important types of defects in TMDCs, point defect and grain boundary, and their influence on the electronic band structure in different conditions. There is no gainsaying that defects caused by intentional doping and etching could modulate the electrical and magnetic properties [40–42], and some significative defect designs are also beneficial to promote in-depth defect research [43, 44]. For all that, defects are not ideal for TMDCs electronic device applications

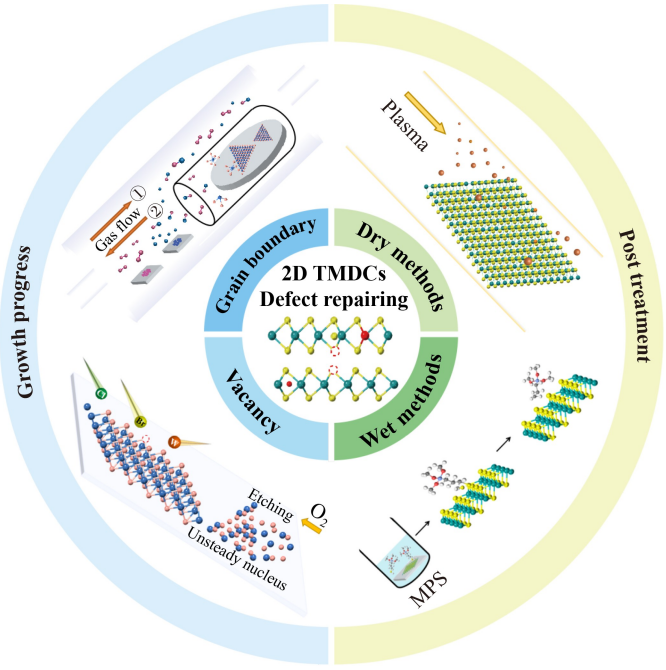

Fig. 1 The scope of this review.

which have a strict requirement for the crystallinity to ensure high carrier mobility. Subsequently, we focus on some highly efficient methods suppressing defects during the process of synthesis. Despite various synthetic methods, chemical vapor deposition (CVD) is one of the most commonly used methods for low cost, simple operation, short growth cycle and large area preparation [45–47], while TMDCs grown by CVD usually produce chalcogen vacancies and grain boundaries [48]. Hence, the assistance of halide, oxide and oxygen plasma aiming to control the vacancy generation and the selection of parameter, source, substrate as well as pretreatment and additive in allusion to grain boundary suppression are described respectively. Afterwards, we summarize the post-treatment strategies with dry and wet methods for representative chalcogen vacancies since defects cannot be eliminated completely during the growth. Interestingly, plasma with different gas and annealing in appropriate atmosphere could have a prominent effect on lowering the defect concentration by one or two order of magnitude, and thus the device properties are improved multiply. At last, we make a conclusion and put forward assumption and prospective for defect engineering in 2D TMDCs, which could provide a wider applied fields for TMDCs and inspire researches of other 2D materials.

2 Defect types

2.1 Point defect

As the simplest kind of crystal defects, point defects are also considered as defects in zero dimension owing to their small size at arbitrary direction in three dimensions [49]. Those defects are deviating from the original arrangement of the crystal structure at the specific position or in the adjacent microscopic region. Familiar types of point defects [50] are shown in Fig. 2(a), including vacancies, adatoms, substitution and interstitial impurities. Notably, vacancy [51] is the most important sort of point defects induced by thermal motion of atoms in the crystal, which is usually arisen during the synthesis process for high temperature. Generally, the vibration energy of atoms rises with the increasing temperature, and will be out of the balanced site when the energy is enough to resist bound energy, leaving isolated vacancies at the lattice site. Just as the Schottky vacancy [52] in Fig. 2(a), a metal vacancy and a chalcogen vacancy have been displayed, while dislocated atoms commonly enter into other vacancies or gradually transfer to the grain boundary or surface. When the atom from the crystal squeezes into the gap between the lattice, another defect called self-interstitial atom will be formed, simultaneously generating a corresponding vacancy. This pair of point defects containing a vacancy and an interstitial atom is Frenkel defect [50] as known. Normally, the concentration of vacancy will increase with the rising temperature on the basis of statistical thermodynamics. In addition, foreign atoms can also be regarded as point defects for changing the normal lattice due to the different atom size and chemical electronegativity. Figure 2(a) also shows the smaller foreign atom could fill an interstice among the host atoms, while the foreign atom with suitable size replaces a host atom, called interstitial atom and substitutional atom respectively. What's more, compared with substitutional and interstitial atoms, the adatom lying on the crystal surface is energetically more favorable to form [53], which is also shown in Fig. 2(a).

Furthermore, when defective points emerging continuously along the edge, a kind of one-dimensional defect called edge is formed [54], which is shown in Fig. 2(b). Those edge defects are generally created to provide active sites for catalysis and can be increased through constructing molecular clusters, nano-particles and other nanostructures. Many researches in catalysis have investigated how to expose more edge sites, so that the catalytic performance will be improved [55].

2.2 Grain boundary

Grain boundary is a typical kind of interfacial defects with two dimensions, which is always existed in polycrystalline materials and separates two small grains of different directions [49]. Due to different grain orientations, grain boundaries are ubiquitous at the interface when films driven by different domains overlap each other during the growth process of large-area TMDCs [56]. According to the angle of misorientation between two neighboring grains, grain boundaries [57] can be divided into low-angle grain boundary and high-angle grain boundary as shown in Fig. 2(c). Apparently, the orientation of grains changes along the boundary, and thus irregular alignments endow the atoms at grain boundary with higher energy than those inside the grains, which could further affect the quality of crystals. Additionally, the energy will enhance following the increasing mismatch angle, since the structure of interface becomes more complicated, and finally lead to higher density and smaller size of domains [58].

It is obvious that defects like vacancies and grain boundaries in the crystal will have a crucial influence on various properties of materials as a result of breaking the regulation of atomic arrangement. Especially, the energy level around the defects differs from that of regular lattice, inducing local energy levels in the forbidden band. In general, the type and concentration of defects could determine the shift of Fermi level [59–61]. Fig. 2(d) shows four situations of the energy level caused by different defects in 2D system. When defects play the role of donor and bring higher electron concentration, the Fermi level will move towards the conduction band. For example, the sulfur vacancies in MoS_2 make the electrons of molybdenum unpaired, thereby turning into free electrons to participate in the conduction process.

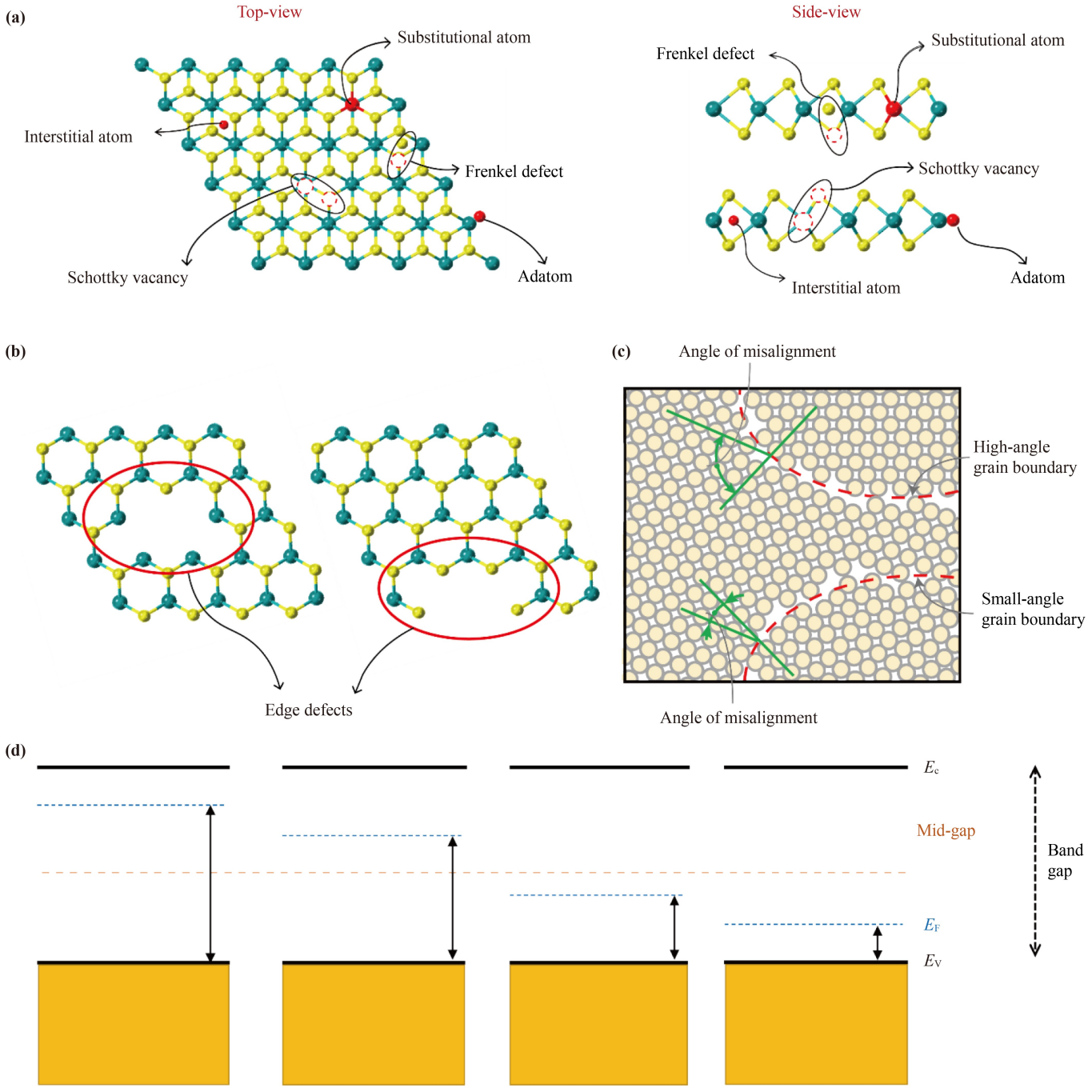

Fig. 2 **(a)** Top view and side view of point defects: Schottky vacancy, Frenkel defect, adatoms, interstitial atom and substitutional atom. **(b)** The diagram of edge defects. **(c)** The diagram of grain boundary: low-angle grain boundary and high-angle grain boundary. **(d)** The occupation of energy levels caused by different defects.

Therefore, the MoS_2 with sulfur vacancies would transform to an n-type semiconductor and the Fermi level representing the intensity of electron filling the energy level will improve [59]. At a certain temperature, the Fermi level is closer to the bottom of the conduction band with the increasement of donor defects. On the contrary, the accepter-like defects will trigger hole conduction and gradually shift the Fermi level near to the valence band in the wake of increasing defect concentration. Ji *et al.* [62] have demonstrated that intrinsic W vacancies in WSe_2 monolayer via STM and *ab initio* calculations are the critical cause inducing p doping, which is completely different from common intrinsic chalcogen vacancies in most TMDCs. With regard to fabricating lateral heterostructure, this p-type doping is always expected but rare to realize [63].

As for 2D TMDCs, their electronic and optoelectronic properties are closely related to the change of band

structure which affects the absorption and emission of light as well as the capture and release of carriers [64]. Undeniably, the defect energy levels introduced in the forbidden band to some extent broaden the photoelectric applications on account of tuning the width of the band gap. However, these defects would inevitably lead to the formation of trap states, which usually reduce the mobility [65]. In consequence, it is necessary to repair the defects through the defect engineering, so that the electrons will turn to extended states and the performance comprising mobility, on/off current ratio, photoresponsivity, etc. will be improved. Furthermore, repairing defects is an effective way to eliminate the boundaries and realize the large-area growth of 2D TMDCs.

3 Improve the quality during the growth

3.1 Vacancy

To reduce the vacancy, one strategy is optimizing the growth condition. Recently, Wang *et al.* [66] proposed a novel method to grow MoS_2 by introducing sodium halide NaX (X = Cl, Br and I) during the growth as shown in Fig. 3(a). The results show that the sodium halide would not only facilitate the growth of the MoS_2 domain, but also suppress the excitons bound originating from the sulfur vacancy. By theoretically calculation, it was demonstrated that the X atoms would absorb at sulfur vacancy, and then passivated it and eliminate the trapping states. Moreover, introduced other metallic oxide powder as the blended precursor is also an effective strategy to decrease nonmetallic vacancy [67–69]. Li *et al.* [70] introduced few WO_3 as mixed precursor with MoO_3 during the preparation of CVD-grown $MoSe_2$, achieving the isoelectronic doping of W atoms in monolayer $MoSe_2$. Eventually, the $Mo_{0.98}W_{0.02}Se_2$ and $Mo_{0.82}W_{0.18}Se_2$ were obtained at the different weight ratio of WO_3/MoO_3. According to Fig. 3(b), the HAADF-STEM measurement, the relative content of Se vacancy decreased from 4% to 2.5%, and 4% to 2% for $Mo_{0.98}W_{0.02}Se_2$ and $Mo_{0.82}W_{0.18}Se_2$ respectively,

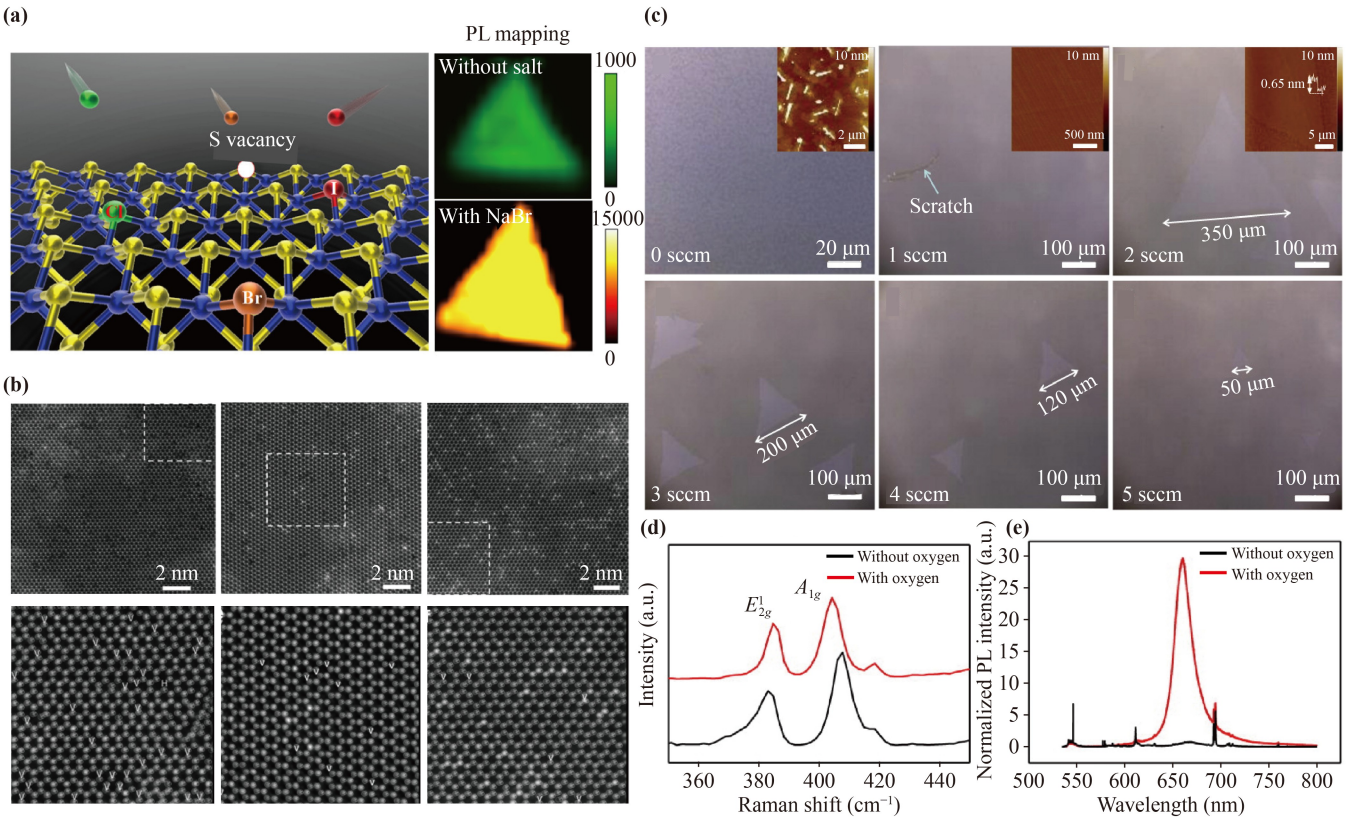

Fig. 3 **(a)** Schematic illustration of the CVD setup for the NaX-assisted (X = Cl, Br, and I) MoS_2 growth, and Raman intensity mappings in two types of MoS_2 samples with NaBr and without salt [66]. **(b)** Large area HAADF-STEM images of $MoSe_2$, $Mo_{0.98}W_{0.02}Se$, and $Mo_{0.82}W_{0.18}Se_2$ monolayers from left to right, respectively (above). Enlarged HAADF-STEM images from the regions contained by dashed squares in corresponding images above after Lucy–Richardson deconvolution (below). The Se vacancies with one missing Se atoms are labeled by V, and those with two missing Se atoms are labeled by H [70]. **(c)** Optical images of MoS_2 grown on sapphire for 30 min with O_2 flow rate ranging from 0 to 5 sccm. The insets are AFM height images of MoS_2 grown on sapphire under different O_2 flow rates (0–2 sccm) [71]. **(d, e)** Typical Raman (d) and photoluminescence (e) spectra of as-grown MoS_2 with (red) and without (black) O_2 carrier gas, respectively [71].

compared to $MoSe_2$, which can be ascribed to the doping W atoms and interpreted by a stronger hybridization between the outermost p orbitals of Se and the d orbitals of W. The PL intensity of $Mo_{0.82}W_{0.18}Se_2$ augmented more than 10 times as compared to pristine $MoSe_2$ because the defect-mediated nonradiative recombination reduced as the reduction of Se vacancy. For obtaining MoS_2 with large area and high crystal quality, Chen *et al.* [71] adopted oxygen-assisted CVD to prepare monolayer MoS_2. As shown in Figs. 3(c–e), the domain size of MoS_2 can reach up to 350 μm and rarely S vacancies was observed. Significantly, the FET property performed excellent with mobility up to 90 $cm^2 \cdot V^{-1} \cdot s^{-1}$. They speculated the oxygen can not only prevent the poisoning of precursors, but also eliminate defects during the growth.

3.2 Grain boundary

In order to reduce the density of grain boundary during the growth of TMDCs, many studies based on the optimization of the growth strategy have conducted to obtain larger domain size. Wang *et al.* [72] achieved a novel two-stage space confinement effect during CVD-growth of monolayer WS_2 as shown in Fig. 4(a), where the stacked substrates formed the micro-reactors for the first stage and substrates placed in another one-side sealed tube for the second stage. As demonstrated in Fig. 4(b), small size and overlap manner of monolayer WS_2 crystals were obtained without these two space confinement effects, while the crystals size was around 100 μm and even up to 450 μm with the first stage and these two stages respectively. Similarly, Tu *et al.* [73] achieved larger grain size, uniform MoS_2 monolayers via CVD method using a double-tube system with one-side sealed inner tube. Other than above strategies, Chen *et al.* [74] developed a two-stage CVD method to prepare MoS_2 monolayers where the induction stage was separated from the growth stage and obtained larger domain size of 305 μm compared to the one-stage CVD method.

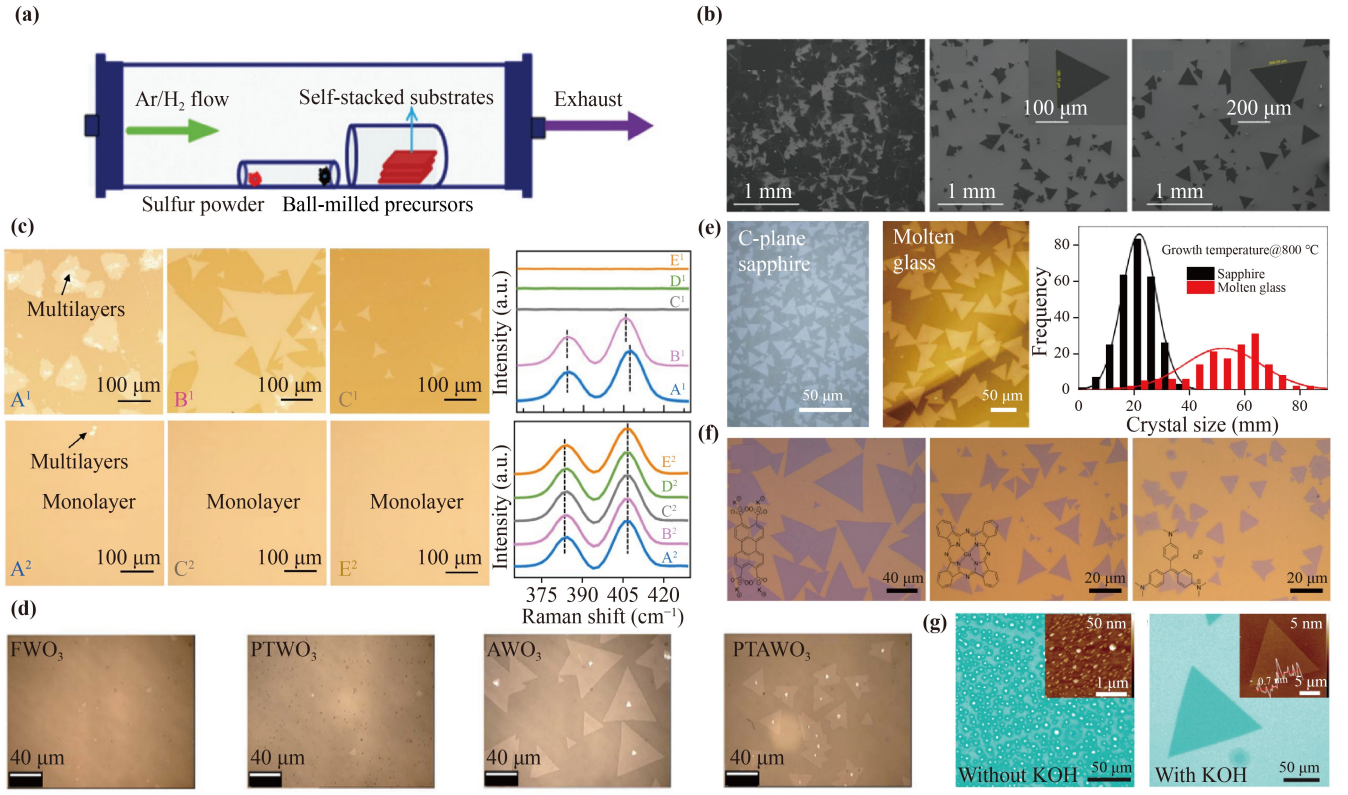

Fig. 4 **(a)** Schematics of the improved CVD synthesis for the high-throughput growth of submillimeter monolayer TMDC single crystals [72]. **(b)** SEM images of WS_2 crystals: on the substrate without self-stacking, on the self-stacked substrate for forming micro-reactors, and on the self-stacked substrate placed in the circumfluence CVD chamber, respectively. The insets show the typical WS_2 flakes correspondingly [72]. **(c)** Corresponding OM images and Raman spectra of MoS_2 synthesized using MoO_3 powder (above) and Mo foil (below) as precursors [79]. **(d)** Optical images of the monolayer WS_2 crystals that were grown from FWO_3, $PTWO_3$, AWO_3, and $PTAWO_3$ powders, respectively [80]. **(e)** Optical microscopy images and domain size distribution histogram of MoS_2 grown on c-plane sapphire and molten glass, respectively [81]. **(f)** Typical optical images of monolayer MoS_2 assisted grown by three different seeding promoters corresponding to PTAS, CuPc and CV, respectively [95]. **(g)** OM and AFM images of MoS_2 grown on SiO_2 without –OH (left) and with –OH (right), respectively [98].

Both of them reduced the nucleation density effectively. Moreover, adjustment of the growth parameter, such as variety, flux and scale of carrier gas [71, 75, 76], the distance between substate and source [77], and the orientation of substrate [78], can achieve the improvement of the domain size.

Selection of the substrate and source also greatly influences the domain size. Yang *et al.* [79] adopted a Mo foil placed above the soda-lime glass growth substrate as the source and obtained highly uniform MoS_2 monolayers with domain size of more than 400 μm, much larger than the power source with 40 μm, which is shown in Fig. 4(c). Pam *et al.* [80] treated WO_3 precursor with different method, including thermal annealing (AWO_3), air plasma ($PTWO_3$), both ($PTAWO_3$) and commercially available WO_3 powder (FWO_3). As shown in Fig. 4(d), the AWO_3 obtained the largest domain size. In addition to the source, Zhang *et al.* [81] implemented large-size high quality MoS_2 monolayer with domain size up to 563 μm on molten glass, which was 3 times larger than the sapphire substrate. The result is shown in Fig. 4(e) clearly. Significantly, corresponding mobility and on/off ratio of MoS_2-based FET were 20 times and two orders of magnitude higher than that transferred from sapphire, respectively. Even 2.5-millimeter single-crystal $MoSe_2$ monolayer was achieved on molten glass [82]. Besides, large domain size of TMDCs films up to several hundred micrometers can be obtained on Au substrate [83–86]. Godin *et al.* [87] adopted substrates pretreated by oxygen plasma. Compared to nontreatment substrate, the average grain size increased by 78% from 56 μm^2 to 101 μm^2, which can be ascribed to lowered activation energy for growth and increased lateral diffusion on the substrate.

Catalysts and additives are increasingly used to produce TMDCs films with higher quality, such as alkali metal compound [88–94], PTAS [95, 96] and other additives [97–99]. Huan *et al.* [93] developed a NaCl-assisted CVD method. Consequently, they obtained larger MoS_2 monolayers with domain size of 100 μm, much larger than 100 nm without the assist of NaCl. Moreover, the triangular MoS_2 domain can up to 300 μm through the optimization of growth parameter. Significantly, fast growth of large-domain MoS_2 monolayers was achieved with a growth rate ~5 $\mu m \cdot s^{-1}$. Furthermore, studies showed that the growth system using NaCl as catalyst can obtain TMDCs thin films with crystal domain size of 632 μm [89] or even 1.7 mm [88]. Yang *et al.* [95] adopted different seeding promoters (PTAS, CuPc and CV) to explore their different influence on the CVD-grown MoS_2 monolayers. As shown in Fig. 4(f), PTAS seeding performed best with the largest domain size of 70 μm while the domain size of MoS_2 with CuPc and CV was between 10 and 20 μm. Besides, the mobility of PTAS-assisted MoS_2 was 23.2 $cm^2 \cdot V^{-1} \cdot s^{-1}$ and the current on/off ratio was 10^6–10^7. It can be explained by the presence of PTAS possibly increased the surface adhesive force of MoS_2, resulted in the layered growth of MoS_2. Interestingly, Zhang *et al.* [98] introduced hydroxide mixed with ammonium molybdate to form aqueous solution as Mo source to prepare MoS_2 monolayer. Eventually, as seen in Fig. 4(g), MoS_2 monolayers grown with –OH possessed larger domain size of 200 μm than system without –OH of 500 nm, where the –OH groups were attached to the (001) surface of MoS_2, forming a MoS_2–OH bilayer structure. The surface –OH layer not only suspended the growth along the [001] axis and led to preferential growth of MoS_2 monolayers, but also protected the MoS_2 surface from oxidation in air. Significantly, the field-effect carrier mobility and on/off current ratio were 30 $cm^2 \cdot V^{-1} \cdot s^{-1}$ and 10^7, respectively.

4 Improve the quality by post-treatment

4.1 Sulfur vacancy

4.1.1 Post-treatment by dry method

To solve the limitation of TMDCs application in the field of electronic devices, which is caused by intrinsic defects, mostly the sulfur vacancies, besides repair methods during growth, many post-treating methods have been conducted. Jiang *et al.* [100] developed a method as shown in Fig. 5(a), treating the multilayered WS_2 gained by mechanical exfoliation with nitrogen plasma, for repairing the sulfur vacancies. The high-resolution spherical aberration correction STEM images in Fig. 5(b) and the calculation indicated that an average density of sulfur vacancy (Vs) was smaller than pristine samples from 0.181 nm^{-2} to 0.049 nm^{-2}, which was induced by the N atoms adsorption at sulfur vacancies and the formation of W–N bonds. Furthermore, because of the nitrogen plasma treatment, the performance of WS_2 FETs enhanced obviously, with the field-effect mobility increased from 29.7 to 184.2 $cm^2 \cdot V^{-1} \cdot s^{-1}$ and the on/off current ratio increased by three orders of magnitude. There are many other approaches with similar repair mechanisms where these vacancies were boned with other atoms. Nan *et al.* [101] adopted post-treatment to exfoliated MoS_2 films with mild oxygen plasma and achieved controllable defect concentration particularly S vacancy in MoS_2. Eventually, the PL intensity increased by nearly 100 times, by which O atoms can chemisorb on S vacancy and achieve the p-type doping. Pierucci *et al.* [102] treated monolayer MoS_2 grown by CVD with hydrogen, as represented in Fig. 5(c), and the XPS measurement displayed gradually decrease of the substoichiometric signature peak owe to Mo atoms around S vacancy, from 18% to 13%, even nearly disappeared as the increased dose of hydrogen compared to pristine MoS_2. The decrease of S vacancy can be explained by the partial saturation of these vacancies with hydrogen

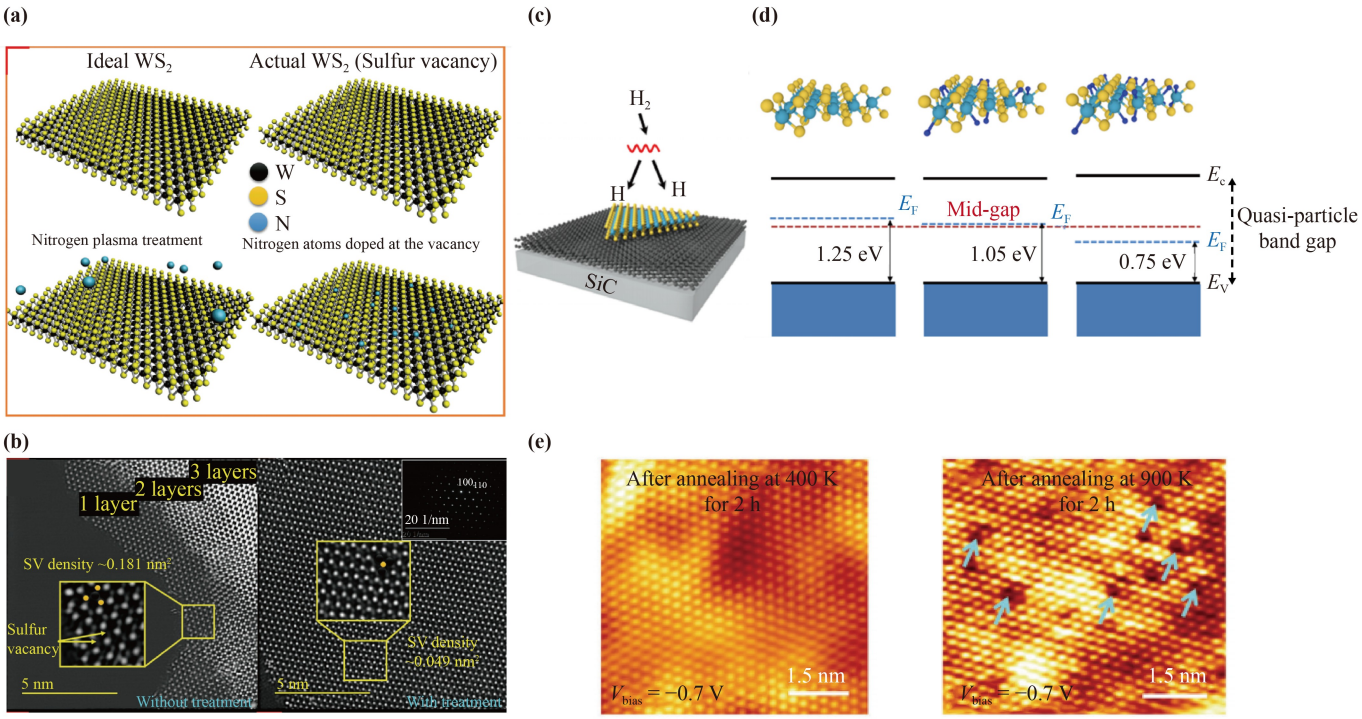

Fig. 5 **(a)** A 3D schematic plot of layered WS_2, with the sulfur atoms shown in yellow, tungsten atoms in gray and the N atoms in blue [100]. **(b)** Atomic structures of WS_2 without nitrogen plasma treatment (left) and with nitrogen plasma treatment (right) that were obtained via STEM. The insets are schematic diagram of sulfur atom (yellow round) and tungsten atom (brown round), as well as the corresponding SAED pattern [100]. **(c)** Schematic illustration of for hydrogen-doped MoS_2 [102]. **(d)** Band diagram showing the evolution of MoS_2 Fermi level: before hydrogenation, upon the first exposure to hydrogen, and after the complete hydrogenation, respectively [102]. **(e)** STM images of MoS_2/G/Au after annealing at different temperature [105].

atoms forming Mo–H bonds, as shown in Fig. 5(d). Significantly, the conversion of electronic properties of monolayer MoS_2 was achieved from the intrinsic electron (n) to hole (p) doping after hydrogen treatment.

Besides the introduction of foreign atoms to form chemical bonds, annealing in the same atmosphere can also achieve the purpose of vacancy repair [103–105]. Liu *et al.* [105] annealed CVD-grown MoS_2 monolayers under ultrahigh vacuum conditions at different temperature, which is shown in Fig. 5(e), and obtained nearly defect-free films with lower defect concentration of 1.2×10^{11} cm^{-2} after annealing at 400 K compared to the usual value of 10^{13} cm^{-2}. Moreover, laser irradiation also can repair nonmetallic vacancy effectively and enhance PL intensity eventually [106–108].

4.1.2 Post-treatment by wet method

There are many kinds of solution treatment which can also achieve defect repair through the mechanism that vacancies were filled by foreign atoms to form chemical bonds. Recently, bis-(trifluoromethane) sulfonimide (TFSI) treatment shows excellent vacancy repair potential [109–116]. Dai *et al.* [110] reported the chemical method treated by bis-(trifluoromethane) sulfonimide (TFSI) to repair the S vacancies in monolayer CVD-grown MoS_2 and WS_2. After the treatment, the XPS spectra of MoS_2 shows the increase of S/Mo ratio from 1.532 to 1.832, so as to indicate successful defect repair of Vs. The PL intensity enhanced nearly 50 times. Amani *et al.* [114] obtained similar results as shown in Fig. 6(a), where the S/Mo ratio increased from 1.84 to 1.95 compared to as-exfoliated MoS_2 and PL intensity enhanced over two orders of magnitude and photoluminescence quantum yield increased from 0.6% to 95% after the treatment of TFSI. Roy *et al.* [111] conducted the same study and the ADF-STEM images in Fig. 6(b) showed that there was an obvious reduction of the Vs and V_{S2}'s relative content in MoS_2 from 2.65% to 0.32% and 0.27% to 0.1% after TFSI treatment respectively, confirming the success of the defect repair. Significantly, they revealed the mechanism of the repair is that S vacancy sites were directly filled by the excess S atoms supplied by the TFSI molecules. Moreover, Dhakal *et al.* [112] confirmed the vacancy repair effect of TFSI through different enhancement of photoluminescence intensity in different regions of MoS_2. The results displayed that Raman intensity ratio of the 2LA(M) and A_{1g} peaks, where a smaller value of ratio indicates more defects, enhanced from 3.8 to 5.4 at the edge, while 3.8 to 4.7 in the center

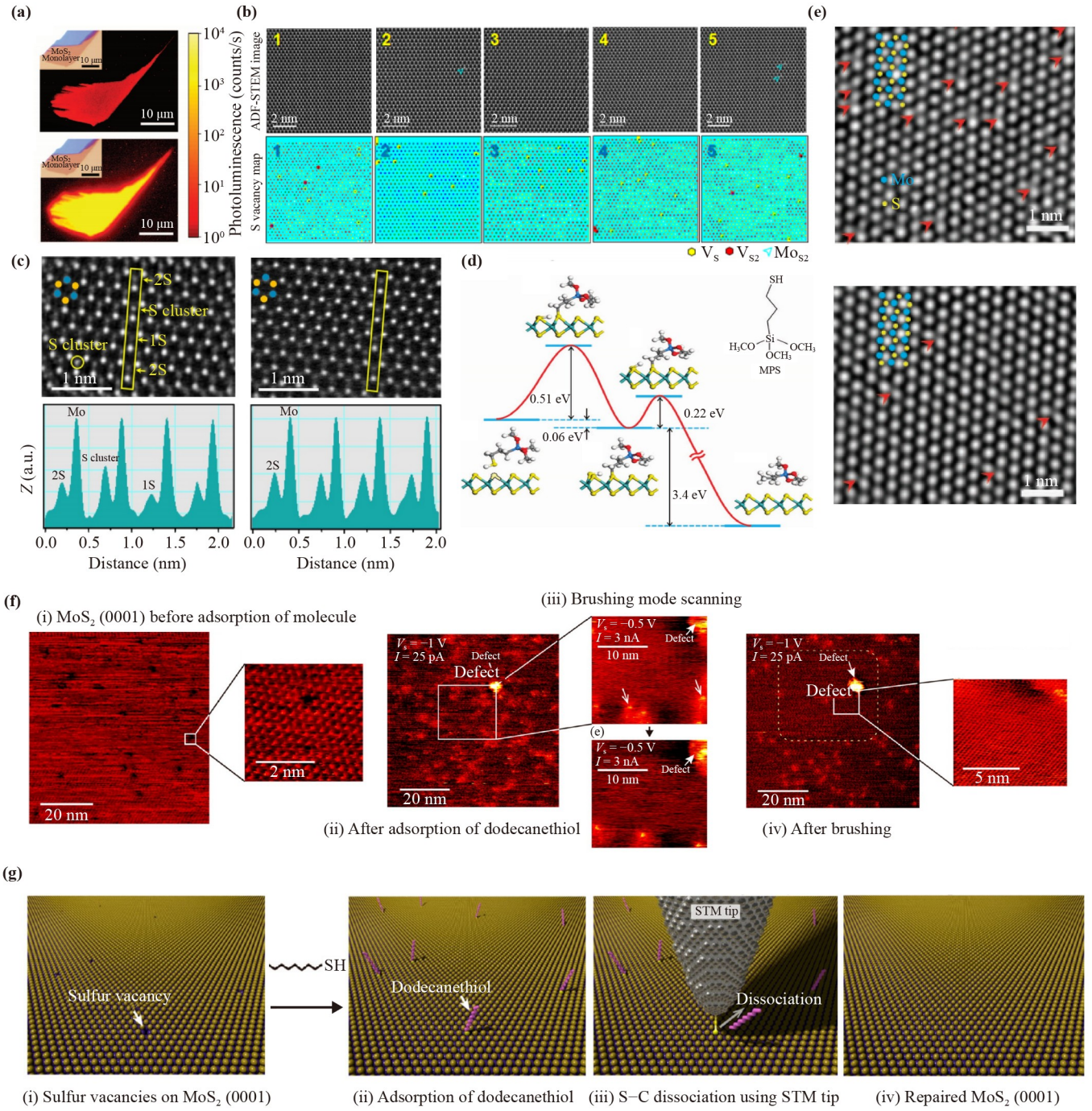

Fig. 6 **(a)** PL images of a MoS_2 monolayer before (above) and after treatment (below). Insets show optical micrographs [114]. **(b)** ADF-STEM images of five pristine 1L-MoS_2 samples (top panels) and the distribution maps (bottom panels) of the V_S (yellow dot) and V_{S2} (red dot) defects measured from the corresponding ADF-STEM images. Note that a noticeable antisite defect, Mo_{S2}, is observed and is denoted by an arrow on the ADF-STEM images [111]. **(c)** The HAADF images and *Z*-contrast mapping in the areas marked with yellow rectangles before (left) and after (right) PSS-induced SVSH, reveal that the sulfur vacancies (1S) are healed spontaneously by the sulfur adatom clusters on MoS_2 surface through a PSS-induced hydrogenation process [118]. **(d)** Kinetics and transient states of the reaction between a single SV and MPS. There are two energy barriers, the first one (0.51 eV) is due to the S–H bond breaking, and the second one (0.22 eV) is due to S–C bond breaking. The inset shows the chemical structure of MPS [120]. **(e)** High-resolution aberration-corrected TEM images of as-exfoliated (left) and TS-treated (right) monolayer MoS_2 sample, showing the significant reduction of SV by MPS treatment. The SVs are highlighted by red arrows. The overlaid blue and yellow symbols mark the position of Mo and S atoms, respectively [120]. **(f)** Series of STM images of MoS_2 (0001) surface before and after adsorption of dodecanethiol molecules [123]. **(g)** Schematic of probable repairing processes [123].

after the TFSI treatment. According to previous research, there were more S vacancies at the edge of 1L-MoS_2 than inner region, which indicated why more effective improvement occurred at the edge. Namely, it was further proved the chemical treatment with TFSI can repair S vacancies in 1L-MoS_2 effectively.

Besides the TFSI, poly(4-styrenesulfonate) (PSS) has also been employed to repair the TMDCs. It was found in Fig. 6(c) that the PSS treatment would decrease the sulfur vacancy. It was reported the S/Mo ratio of MoS_2 had a remarkable increase from 1.67 to 1.86 after PSS treatment. The electron concentration would decrease by 643 times. Furthermore, the PL intensity and photoresponsivity which reaches up to 339.2 $A \cdot W^{-1}$, increased about 2-fold and 5.6-fold respectively after the treatment [117, 118]. Zhang *et al.* [119] found that the PSS treatment would improve the stability of the MoS_2 in air, where after exposure 12 months, the property has no obvious decay.

Similarly, thiol molecules can adsorb on S vacancies of TMDCs and complete defect repair. It was studied that (3-mercaptopropyl)- trimethoxysilane(MPS), a kind of thiol molecules, can repair S vacancies through two steps. The detailed reaction is shown in Fig. 6(d). Firstly, S atom in MPS chemisorbed onto a defect site of S vacancies, with the fracture of S–H bond. Secondly, the S–C bond broke and the S vacancy was repaired thoroughly with the formation of byproduct trimethoxy(propyl)silane. Significantly, as illustrated in Fig. 6(e), the density of S vacancy has decreased from 6.5×10^{13} cm^{-2} to 1.6×10^{13} cm^{-2} and the S/W ratio increased obviously from 1.62 to 1.98 after the MPS treatment. Besides, the FET mobility enhanced from 40 $cm^2 \cdot V^{-1} \cdot s^{-1}$ to 80 $cm^2 \cdot V^{-1} \cdot s^{-1}$ [120, 121]. Similarly, the S vacancy density decreased from 3% to 1.2% after the butanethiol ($C_4H_{10}S$) treatment, with the augment of the I_{ON}/I_{OFF} ratio and the field-effect mobility from 2×10^6 to 4×10^7 and 1.4 to 8.0 $cm^2 \cdot V^{-1} \cdot s^{-1}$ respectively [122]. Makarova *et al.* [123] exploited thiol molecules to adsorb on S vacancies in MoS_2 and repair these vacancies by the auxiliary effect with the STM tip. The series of STM images in Fig. 6(f) displayed that pristine MoS_2 had some darker points which are the S vacancies, however, it got to be bright after the adsorption of thiol molecules. Significantly, after removal of the alkyl by the brushing of the STM tip, the darker points disappeared. All the results indicated the effective repair of S vacancies, and the probable repairing processes are shown in Fig. 6(g). Moreover, it was reported that PL intensity and electrical performance of MoS_2-based FET would be improved after the treatment of thiol molecules with the field-effect mobility enhanced by 3 times [124–126]. Furthermore, thiol-based organic compounds with different functional group could achieve different types of doping, n-type doping and p-type doping [127].

There are many other chemical reagents available for vacancy repair, such as ethylene diamine tetraacetic acid (EDTA) [128], titanyl phthalocyanine (TiOPc) [129], $CuCl_2$ [130], oleic acid (OA) [131], Ag-NPs (Nanoparticles) [132], ionic liquid [133], Protoporphyrin (H2PP) [134], N,N'-ditridecylperylene-3,4,9,10-tetracarboxylic diimide (PTCDI-C13) [135], 2,3,5,6-tetrafluoro-7,7,8,8-tetracyanoquinodimethane (F4TCNQ) and 7,7,8,8-tetracyanoquinodimethane (TCNQ) [136], 1, 2-dichloroethane (DCE) [137], which can enhance the mobility [128, 130, 131, 135], the on/off ratio [129, 137], and the PL intensity [131–133].

4.2 Selenium vacancy repair

4.2.1 Post-treatment by dry method

As a kind of TMDCs, repairing selenium vacancy of selenide would heavily improve its photoelectrochemical properties. Many studies developed an oxygen passivization where the oxygen chemisorbed onto the Se vacancies in monolayer CVD-grown WSe_2. After this treatment, the height of WSe_2 flakes increases for the presence of oxides which is shown in Fig. 7(a), and the XPS results display the peaks contributed to the W–O, namely confirmed the chemisorption of oxygen in WSe_2. Significantly, the W^{4+}/Se ratio increased from 1:1.81 to 1:1.94 and 1:2.06 after laser passivization in vacuum and ambient conditions respectively. Moreover, it was experimentally confirmed that the Se vacancies passivization by oxygen enhanced the conductivity and photoconductivity of monolayer WSe_2 respectively by 400 times and 150 times [138]. Moreover, Wang *et al.* [139] developed one similar strategy shown in Fig. 7(b) to conduct laser annealing on fewer layer $MoSe_2$. The XPS measurement displayed obvious increase of Se/Mo^{4+} ratio from 1.69 to 1.84 after annealing. Meanwhile, the PL and Raman peak intensity both improved. Significantly, light-to-energy conversion efficiency of $MoSe_2$-based electrochemical cell increased by 110%–280%.

4.2.2 Post-treatment by wet method

Similar to the methods of sulfur vacancy repair, some chemicals can also be used to repair selenium vacancies. It was reported that the ratio of the Se to Mo atoms of layered $MoSe_2$ grown by chemical vapor deposition had a significant increase from 1.68 to 1.97 after the treatment of hydrohalic acid like HBr. Significantly, there was over 30 times improvement of PL intensity contributed to the repair of Se-related defects as shown in Fig. 7(c), through the synergistic effect from Br atoms and the conversion of the bridging Se_2^{2-} to the Se^{2-} [140]. Meng *et al.* [141] treated the monolayer $MoSe_2$ grown by CVD method with EDTA for healing the defect such as Se vacancy in $MoSe_2$. The FET based on single layer $MoSe_2$

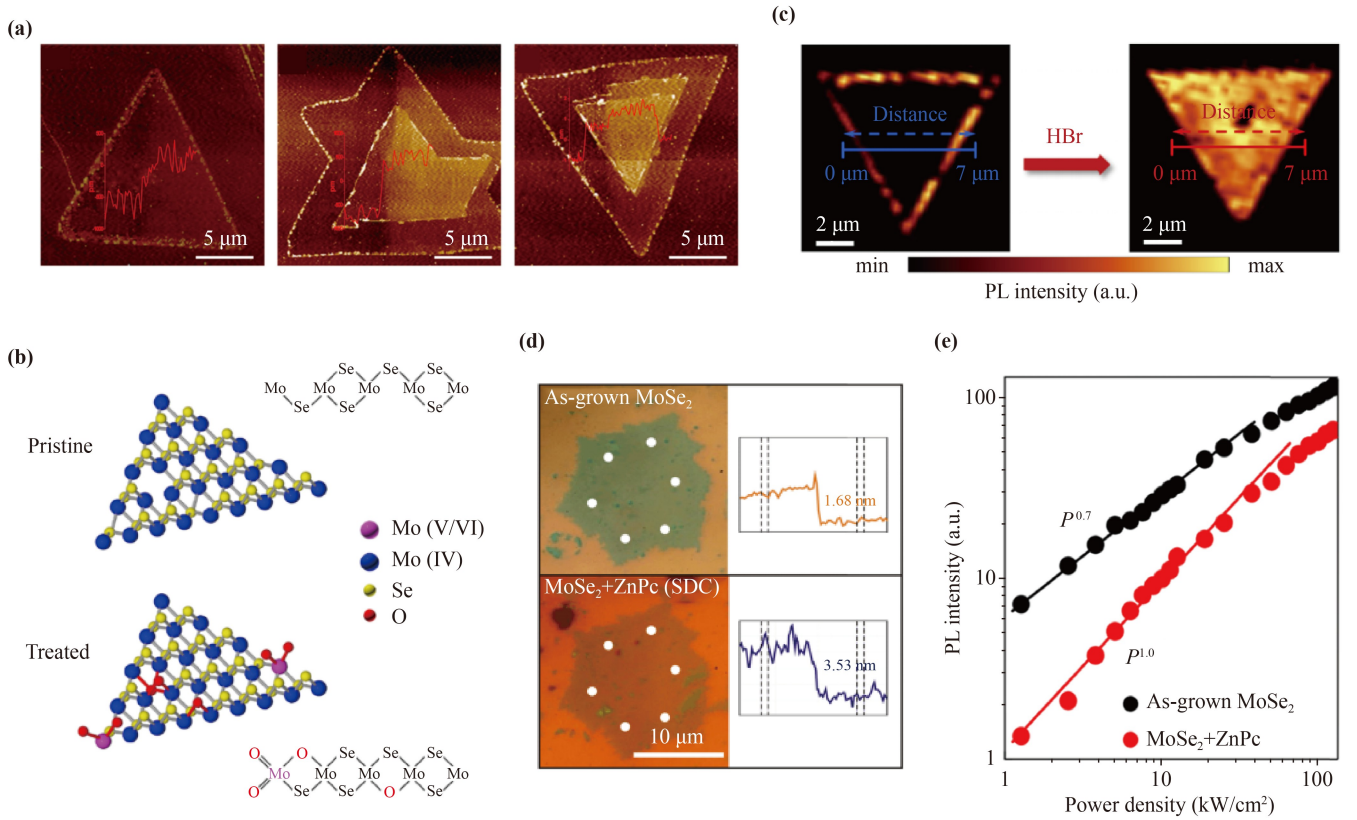

Fig. 7 **(a)** AFM characterization of partially laser modified WSe_2 flakes. For each of these flakes, the portion on the right corresponds to laser modified region. **(b)** Proposed photo-induced chemical changes to the $MoSe_2$ sample. **(c)** PL intensity mappings of an individual $MoSe_2$ flake before and after HBr treatment. **(d)** Optical microscopic images of $MoSe_2$ flakes on SiO_2/Si (upper panel) and those of the same flakes after the deposition of ZnPc by SDC methods (lower panel). The second column shows the thickness of the as-grown and functionalized $MoSe_2$ using the SDC method, analyzed by AFM. **(e)** PL intensity as a function of the excitation power for as-grown $MoSe_2$ and $MoSe_2$ + ZnPc.

device's electronic mobility gains about 300 times from 0.1 $cm^2 \cdot V^{-1} \cdot s^{-1}$ to 30 $cm^2 \cdot V^{-1} \cdot s^{-1}$ and hole mobility over 10 $cm^2 \cdot V^{-1} \cdot s^{-1}$. Besides, coating the CVD-grown $MoSe_2$ with ZnPc which is a kind of organic dopants named MPc was demonstrated a simple method to passivate the Se-vacancies, which has been demonstrated in Figs. 7(d) and (e), where ZnPc bonded by van der Waals on the surface of TMDCs can reduce the defect density effectively for absorbing at the Se-vacancies in $MoSe_2$ [142].

Table 1 has summarized recent researches of defect repairing in CVD-grown TMDCs. Different strategies for undesirable vacancies and grain boundaries effectively improve the performance of TMDCs, including the carrier mobility, on/off current ratio, PL intensity, etc. In particular, large-area grown TMDCs are gradually realized by controlling the domain density during the growth to reduce grain boundaries, which is expected to meet the industry demand.

5 Conclusion and outlook

In recent years, two-dimensional layered TMDCs with unique atomic structure have attracted extensive attentions for breaking the zero-band gap limitation of graphene. Abundant band structures depending on thickness give them a wide range of electrical properties which have covered metals, semiconductors and even superconductors. Hence, TMDCs are expected to achieve the controllable property manipulation and the emerging application extension in the field of electronics, optoelectronics, biosensors, catalysis, and so forth. Up to now, a large number of experimental results and theoretical calculations have shown that the lattice defects play a key role in the optical and electrical properties of TMDCs [143]. Accordingly, researchers have made significant efforts to study the defect repairing for the sake of performance modification in all kinds of TMDCs. In this review, we have emphasized key developments in defect engineering of 2D layered TMDCs, mainly focusing on (i) the repair methods of vacancies and grain boundaries during the CVD growth process, such as appropriate additive introduction, oxygen plasma assistance and growth procedure design. Other than that, (ii) the post treatment aiming at the non-metallic defects in synthesized films like S vacancy and Se vacancy and their influence

Table 1 Summary of important defect repairing methods in TMDCs.

Defect type	Repair stage	Properties	Repairing method	Refs.
Sulfur vacancies	Growth process	N-type doping	Introducing NaX	[66]
		Lower mobility	Oxygen-assisted CVD	[71]
	Post-treatment	Lower on/off current ratio	N_2, O_2, H_2 plasma treatment	[100–102]
			Annealing	[105]
		Weaker PL intensity	TFSI treatment	[110]
			PSS treatment	[119]
			MPS treatment	[120]
Selenium vacancies	Growth process	N-type doping	Introducing other metallic oxide powder	[70]
	Post-treatment	Weaker PL intensity	Oxygen passivization	[138]
			Annealing	[139]
			HBr treatment	[140]
		Lower mobility	MPc treatment	[135]
Grain boundaries	Growth process	Higher domain density Small size	Space confinement effect	[72]
			Double-tube system with one-side sealed inner tube	[73]
			Two-stage (induction and growth stage) CVD method	[74]
		Lower mobility Lower on/off current	Selection and pretreatment of the substrate and source	[79–81]
			Introducing catalysts and additives	[88–99]
	Post-treatment	–		

are comprehensively discussed from both dry and wet methods perspectives. Annealing, plasma and special solution treatment, such as TFSI, PSS, and HBr, are all effective to reduce the undesirable defects in TMDCs and enhance their electrical performance. Nevertheless, there are still plenty of challenges to surmount in the future study on defect engineering as follow.

5.1 Revealing defect repairing mechanism

To date, few kinds of ultra-thin wafer-scale TMDCs are realized due to grain boundaries which could impede their epitaxial growth. On top of that, vacancy is also a crucial factor to consider in the defect engineering, which could hinder the high-performance electronic devices. Current researches have studied how to diminish those unwished defects generated during the synthesis through growth parameter alteration and how to repair the inherent defects of as-grown TMDCs by post-treatment. However, the repair mechanism is ambiguous in the present and the performance enhancement is limited and uncontrollable. On one hand, the exhibited properties of TMDCs are influenced by many parameters including the distance between the source and substrate, the flow rate, the ambient pressure, etc. On the other hand, considering the wide variety of TMDCs, it is complicated to precisely tailor the growth parameters corresponding to different types. Therefore, further researches should focus on exploring the specific defect repairing mechanism and the synthetic mechanism of 2D TMDCs, so that people could control their size and orientation more accurately in essence.

5.2 Optimizing repairing process design

Although repairing methods via plasma irradiation and chemical treatment are two promising avenues to solve the deficiency in TMDCs, there are still some problems existed like increasing energy consumption and tail gas in the dry methods, as well as unavoidable to introduce contamination and other defects in the wet methods. Thus, defect repairing process optimization ensuring the low defect density is required for the prospective defect engineering to improve the conductivity and photoconductivity. Meanwhile, both efficiency and cost of defect repairing are also needed to consider in the design. In this way, we can predict that the progressive development of defect engineering in the near future will make a major stride toward electrical, optoelectronic, magnetic and spin electronic applications.

Acknowledgements This work was financially supported by the National Natural Science Foundation of China (Nos. 52002254 and 52272160), the Sichuan Science and Technology Foundation (Nos. 2020YJ0262, 2021YFH0127, 2023YFSY0002, and 2022YFS0045), the Chunhui Plan of the Ministry of Education, Fundamental Research Funds for the Central Universities, China (No. YJ201893), and the Open-Foundation of Key Laboratory of Laser Device Technology, China North Industries Group Corporation Limited (Grant No. KLLDT202104).

References

1. A. K. Geim, Graphene: Status and prospects, *Science* 324(5934), 1530 (2009)
2. K. S. Novoselov, V. I. Fal'ko, L. Colombo, P. R.

Gellert, M. G. Schwab, and K. Kim, A roadmap for graphene, *Nature* 490(7419), 192 (2012)
3. K. M. Wyss, D. X. Luong, and J. M. Tour, Large-scale syntheses of 2D materials: Flash Joule heating and other methods, *Adv. Mater.* 34(8), 2106970 (2022)
4. J. Li, M. Chen, A. Samad, H. Dong, A. Ray, J. Zhang, X. Jiang, U. Schwingenschlögl, J. Domke, C. Chen, Y. Han, T. Fritz, R. S. Ruoff, B. Tian, and X. Zhang, Wafer-scale single-crystal monolayer graphene grown on sapphire substrate, *Nat. Mater.* 21(7), 740 (2022)
5. Y. Zhang, W. Shen, S. Wu, W. Tang, Y. Shu, K. Ma, B. Zhang, P. Zhou, and S. Wang, High-speed transition-metal dichalcogenides based Schottky photodiodes for visible and infrared light communication, *ACS Nano* 16(11), 19187 (2022)
6. L. Hou, X. Cui, B. Guan, S. Wang, R. Li, Y. Liu, D. Zhu, and J. Zheng, Synthesis of a monolayer fullerene network, *Nature* 606(7914), 507 (2022)
7. G. Murali, J. K. R. Modigunta, Y. H. Park, J. H. Lee, J. Rawal, S. Y. Lee, I. In, and S. J. Park, A review on MXene synthesis, stability, and photocatalytic applications, *ACS Nano* 16(9), 13370 (2022)
8. A. E. Naclerio and P. R. Kidambi, A review of scalable hexagonal boron nitride (h-BN) synthesis for present and future applications, *Adv. Mater.* 35(6), 2207374 (2023)
9. Z. Zhang, P. Yang, M. Hong, S. Jiang, G. Zhao, J. Shi, Q. Xie, and Y. Zhang, Recent progress in the controlled synthesis of 2D metallic transition metal dichalcogenides, *Nanotechnology* 30(18), 182002 (2019)
10. H. Ma, Q. Qian, B. Qin, Z. Wan, R. Wu, B. Zhao, H. Zhang, Z. Zhang, J. Li, Z. Zhang, B. Li, L. Wang, and X. Duan, Controlled synthesis of ultrathin $PtSe_2$ nanosheets with thickness-tunable electrical and magnetoelectrical properties, *Adv. Sci. (Weinh.)* 9(1), 2103507 (2022)
11. Y. Wang, J. C. Kim, Y. Li, K. Y. Ma, S. Hong, M. Kim, H. S. Shin, H. Y. Jeong, and M. Chhowalla, P-type electrical contacts for 2D transition-metal dichalcogenides, *Nature* 610(7930), 61 (2022)
12. F. Li, R. Tao, B. Cao, L. Yang, and Z. Wang, Manipulating the light-matter interaction of PtS/MoS_2 p–n junctions for high performance broadband photodetection, *Adv. Funct. Mater.* 31(36), 2104367 (2021)
13. S. Manzeli, D. Ovchinnikov, D. Pasquier, O. V. Yazyev, and A. Kis, 2D transition metal dichalcogenides, *Nat. Rev. Mater.* 2(8), 17033 (2017)
14. L. Pi, L. Li, K. Liu, Q. Zhang, H. Li, and T. Zhai, Recent progress on 2D noble-transition-metal dichalcogenides, *Adv. Funct. Mater.* 29(51), 1904932 (2019)
15. Q. Liang, Z. Chen, Q. Zhang, and A. T. S. Wee, Pentagonal 2D transition metal dichalcogenides: $PdSe_2$ and beyond, *Adv. Funct. Mater.* 32(38), 2203555 (2022)
16. B. Cao, Z. Ye, L. Yang, L. Gou, and Z. Wang, Recent progress in van der Waals 2D $PtSe_2$, *Nanotechnology* 32(41), 412001 (2021)
17. Y. Gao, S. Wang, B. Wang, Z. Jiang, and T. Fang, Recent progress in phase regulation, functionalization, and biosensing applications of polyphase MoS_2, *Small* 18(34), 2202956 (2022)
18. X. Zhu, Y. Chen, Z. Liu, Y. Han, and Z. Qiao, Valley-polarized quantum anomalous Hall effect in van der Waals heterostructures based on monolayer jacutingaite family materials, *Front. Phys.* 18(2), 23302 (2023)
19. Y. Y. Wang, F. P. Li, W. Wei, B. B. Huang, and Y. Dai, Interlayer coupling effect in van der Waals heterostructures of transition metal dichalcogenides, *Front. Phys.* 16(1), 13501 (2021)
20. Q. Liang, Q. Zhang, X. Zhao, M. Liu, and A. T. S. Wee, Defect engineering of two-dimensional transition-metal dichalcogenides: Applications, challenges, and opportunities, *ACS Nano* 15(2), 2165 (2021)
21. Y. Gong, Z. Lin, Y. X. Chen, Q. Khan, C. Wang, B. Zhang, G. Nie, N. Xie, and D. Li, Two-dimensional platinum diselenide:Synthesis, Emerging applications, and future challenges, *Nano-Micro Lett.* 12(1), 174 (2020)
22. E. Norouzzadeh, S. Mohammadi, and M. Moradinasab, Tunneling FET based on defect-free, vacancy-defected, and passivated monolayer $PtSe_2$ channel: A first principles study, *Mater. Sci. Semicond. Process.* 138, 106258 (2022)
23. A. Mahmood, G. Lu, X. Wang, Y. Wang, X. Xie, and J. Sun, Investigating the stability and role of defects in vertically aligned WS_2/MoS_2 heterojunctions on OER activity using first principles study, *J. Power Sources* 551, 232208 (2022)
24. P. M. M. C. de Melo, Z. Zanolli, and M. J. Verstraete, Optical signatures of defect centers in transition metal dichalcogenide monolayers, *Adv. Quant. Technol.* 4(3), 2000118 (2021)
25. Y. Yu, X. Zhang, Z. Zhou, Z. Zhang, Y. Bao, H. Xu, L. Lin, Y. Zhang, and X. Wang, Microscopic pump-probe optical technique to characterize the defect of monolayer transition metal dichalcogenides, *Photon. Res.* 7(7), 711 (2019)
26. K. Wu, H. Zhong, Q. Guo, J. Tang, Z. Yang, L. Qian, S. Yuan, S. Zhang, and H. Xu, Revealing the competition between defect-trapped exciton and band-edge exciton photoluminescence in monolayer hexagonal WS_2, *Adv. Opt. Mater.* 10(6), 2101971 (2022)
27. D. H. Lien, S. Z. Uddin, M. Yeh, M. Amani, H. Kim, J. W. III Ager, E. Yablonovitch, and A. Javey, Electrical suppression of all nonradiative recombination pathways in monolayer semiconductors, *Science* 364(6439), 468 (2019)
28. P. C. Shen, Y. Lin, C. Su, C. McGahan, A. Y. Lu, X. Ji, X. Wang, H. Wang, N. Mao, Y. Guo, J. H. Park, Y. Wang, W. Tisdale, J. Li, X. Ling, K. E. Aidala, T. Palacios, and J. Kong, Healing of donor defect states in monolayer molybdenum disulfide using oxygen-incorporated chemical vapour deposition, *Nat. Electron.* 5(1), 28 (2021)
29. B. Wen, D. N. Luo, L. L. Zhang, X. L. Li, X. Wang, L. L. Huang, X. Zhang, and D. F. Diao, Excited state biexcitons in monolayer WSe_2 driven by vertically grown graphene nanosheets with high-density electron trapping edges, *Front. Phys.* 18(3), 33306 (2023)
30. J. Li, T. Joseph, M. Ghorbani-Asl, S. Kolekar, A. V. Krasheninnikov, and M. Batzill, Edge and point-defect induced electronic and magnetic properties in monolayer

$PtSe_2$, *Adv. Funct. Mater.* 32(18), 2110428 (2022)
31. P. Li, Y. Bu, L. Wang, C. Wang, J. Huang, K. Tong, Y. Chen, J. He, Z. Zhao, B. Xu, Z. Liu, G. Gao, A. Nie, H. Wang, and Y. Tian, *In situ* observation of fracture along twin boundaries in boron carbide, *Adv. Mater.*, doi: 10.1002/adma.202204375 (2022)
32. H. Yun, M. Topsakal, A. Prakash, B. Jalan, J. S. Jeong, T. Birol, and K. A. Mkhoyan, Metallic line defect in wide-bandgap transparent perovskite $BaSnO_3$, *Sci. Adv.* 7(3), eabd4449 (2021)
33. S. Feng, J. Tan, S. Zhao, S. Zhang, U. Khan, L. Tang, X. Zou, J. Lin, H. M. Cheng, and B. Liu, Synthesis of ultrahigh-quality monolayer molybdenum disulfide through *in situ* defect healing with thiol molecules, *Small* 16(35), 2003357 (2020)
34. J. Li, S. Wang, Q. Jiang, H. Qian, S. Hu, H. Kang, C. Chen, X. Zhan, A. Yu, S. Zhao, Y. Zhang, Z. Chen, Y. Sui, S. Qiao, G. Yu, S. Peng, Z. Jin, and X. Liu, Single-crystal MoS_2 monolayer wafer grown on Au(111) film substrates, *Small* 17(30), 2100743 (2021)
35. P. Yang, Y. Shan, J. Chen, G. Ekoya, J. Han, Z. J. Qiu, J. Sun, F. Chen, H. Wang, W. Bao, L. Hu, R. J. Zhang, R. Liu, and C. Cong, Remarkable quality improvement of as-grown monolayer MoS_2 by sulfur vapor pretreatment of SiO_2/Si substrates, *Nanoscale* 12(3), 1958 (2020)
36. F. J. Urbanos, S. Gullace, and P. Samorì, MoS_2 defect healing for high-performance chemical sensing of polycyclic aromatic hydrocarbons, *ACS Nano* 16(7), 11234 (2022)
37. T. Liu, N. Peng, X. Zhang, R. Zheng, M. Xia, H. Yu, M. Shui, Y. Xie, and J. Shu, Controllable defect engineering enhanced bond strength for stable electrochemical energy storage, *Nano Energy* 79, 105460 (2021)
38. G. Chilkoor, N. Shrestha, A. Kutana, M. Tripathi, F. C. Robles Hernández, B. I. Yakobson, M. Meyyappan, A. B. Dalton, P. M. Ajayan, M. M. Rahman, and V. Gadhamshetty, Atomic layers of graphene for microbial corrosion prevention, *ACS Nano* 15(1), 447 (2021)
39. C. Z. Zerger, L. K. Rodenbach, Y. T. Chen, B. Safvati, M. Z. Brubaker, S. Tran, T. A. Chen, M. Y. Li, L. J. Li, D. Goldhaber-Gordon, and H. C. Manoharan, Nanoscale electronic transparency of wafer-scale hexagonal boron nitride, *Nano Lett.* 22(11), 4608 (2022)
40. R. Tao, X. Qu, Z. Wang, F. Li, L. Yang, J. Li, D. Wang, K. Zheng, and M. Dong, Tune the electronic structure of MoS_2 homojunction for broadband photodetection, *J. Mater. Sci. Technol.* 119, 61 (2022)
41. D. Wang, Z. Wang, Z. Yang, S. Wang, C. Tan, L. Yang, X. Hao, Z. Ke, and M. Dong, Facile damage-free double exposure for high-performance 2D semiconductor based transistors, *Mater. Today Phys.* 24, 100678 (2022)
42. K. Fujisawa, B. R. Carvalho, T. Zhang, N. Perea-López, Z. Lin, V. Carozo, S. L. L. M. Ramos, E. Kahn, A. Bolotsky, H. Liu, A. L. Elías, and M. Terrones, Quantification and healing of defects in atomically thin molybdenum disulfide: Beyond the controlled creation of atomic defects, *ACS Nano* 15(6), 9658 (2021)
43. C. Zhang, C. Wang, F. Yang, J. K. Huang, L. J. Li, W. Yao, W. Ji, and C. K. Shih, Engineering point-defect states in monolayer WSe_2, *ACS Nano* 13(2), 1595 (2019)
44. K. Wang, L. Zhang, G. D. Nguyen, X. Sang, C. Liu, Y. Yu, W. Ko, R. R. Unocic, A. A. Puretzky, C. M. Rouleau, D. B. Geohegan, L. Fu, G. Duscher, A. P. Li, M. Yoon, and K. Xiao, Selective antisite defect formation in WS_2 monolayers via reactive growth on dilute W–Au alloy substrates, *Adv. Mater.* 34(3), 2106674 (2022)
45. Z. Gan, I. Paradisanos, A. Estrada-Real, J. Picker, E. Najafidehaghani, F. Davies, C. Neumann, C. Robert, P. Wiecha, K. Watanabe, T. Taniguchi, X. Marie, J. Biskupek, M. Mundszinger, R. Leiter, U. Kaiser, A. V. Krasheninnikov, B. Urbaszek, A. George, and A. Turchanin, Chemical vapor deposition of high-optical-quality large-area monolayer Janus transition metal dichalcogenides, *Adv. Mater.* 34(38), 2205226 (2022)
46. T. Kang, T. W. Tang, B. Pan, H. Liu, K. Zhang, and Z. Luo, Strategies for controlled growth of transition metal dichalcogenides by chemical vapor deposition for integrated electronics, *ACS Mater. Au* 2(6), 665 (2022)
47. Y. Zhang, Y. Yao, M. G. Sendeku, L. Yin, X. Zhan, F. Wang, Z. Wang, and J. He, Recent progress in CVD growth of 2D transition metal dichalcogenides and related heterostructures, *Adv. Mater.* 31(41), 1901694 (2019)
48. Y. Wan, E. Li, Z. Yu, J. K. Huang, M. Y. Li, A. S. Chou, Y. T. Lee, C. J. Lee, H. C. Hsu, Q. Zhan, A. Aljarb, J. H. Fu, S. P. Chiu, X. Wang, J. J. Lin, Y. P. Chiu, W. H. Chang, H. Wang, Y. Shi, N. Lin, Y. Cheng, V. Tung, and L. J. Li, Low-defect-density WS_2 by hydroxide vapor phase deposition, *Nat. Commun.* 13(1), 4149 (2022)
49. A. Hassan, Z. Wang, Y. H. Ahn, M. Azam, A. A. Khan, U. Farooq, M. Zubair, and Y. Cao, Recent defect passivation drifts and role of additive engineering in perovskite photovoltaics, *Nano Energy* 101, 107579 (2022)
50. J. Xu, G. Shao, X. Tang, F. Lv, H. Xiang, C. Jing, S. Liu, S. Dai, Y. Li, J. Luo, and Z. Zhou, Frenkel-defected monolayer MoS_2 catalysts for efficient hydrogen evolution, *Nat. Commun.* 13(1), 2193 (2022)
51. Y. Zuo, C. Liu, L. Ding, R. Qiao, J. Tian, C. Liu, Q. Wang, G. Xue, Y. You, Q. Guo, J. Wang, Y. Fu, K. Liu, X. Zhou, H. Hong, M. Wu, X. Lu, R. Yang, G. Zhang, D. Yu, E. Wang, X. Bai, F. Ding, and K. Liu, Robust growth of two-dimensional metal dichalcogenides and their alloys by active chalcogen monomer supply, *Nat. Commun.* 13(1), 1007 (2022)
52. S. Barja, S. Refaely-Abramson, B. Schuler, D. Y. Qiu, A. Pulkin, S. Wickenburg, H. Ryu, M. M. Ugeda, C. Kastl, C. Chen, C. Hwang, A. Schwartzberg, S. Aloni, S. K. Mo, D. Frank Ogletree, M. F. Crommie, O. V. Yazyev, S. G. Louie, J. B. Neaton, and A. Weber-Bargioni, Identifying substitutional oxygen as a prolific point defect in monolayer transition metal dichalcogenides, *Nat. Commun.* 10(1), 3382 (2019)
53. R. González-Hernández, W. López-Pérez, and J. A. Rodríguez M, Nickel adsorption and incorporation on a 2×2-T4 GaN(0001) surface: A DFT study, *Appl. Surf. Sci.* 266, 205 (2013)
54. T. Tang, Z. Wang, and J. Guan, A review of defect

engineering in two-dimensional materials for electrocatalytic hydrogen evolution reaction, *Chin. J. Catal.* 43(3), 636 (2022)
55. S. Liu, L. Zhou, W. Zhang, J. Jin, X. Mu, S. Zhang, C. Chen, and S. Mu, Stabilizing sulfur vacancy defects by performing "click" chemistry of ultrafine palladium to trigger a high-efficiency hydrogen evolution of MoS_2, *Nanoscale* 12(18), 9943 (2020)
56. M. Cheng, J. Yang, X. Li, H. Li, R. Du, J. Shi, and J. He, Improving the device performances of two-dimensional semiconducting transition metal dichalcogenides: Three strategies, *Front. Phys.* 17(6), 63601 (2022)
57. H. Bishara, S. Lee, T. Brink, M. Ghidelli, and G. Dehm, Understanding grain boundary electrical resistivity in Cu: The effect of boundary structure, *ACS Nano* 15(10), 16607 (2021)
58. J. Zhang, L. Lin, K. Jia, L. Sun, H. Peng, and Z. Liu, Controlled growth of single-crystal graphene films, *Adv. Mater.* 32(1), 1903266 (2020)
59. F. Bussolotti, J. Yang, H. Kawai, C. P. Y. Wong, and K. E. J. Goh, Impact of S-vacancies on the charge injection barrier at the electrical contact with the MoS_2 monolayer, *ACS Nano* 15(2), 2686 (2021)
60. Y. Chen, S. Huang, X. Ji, K. Adepalli, K. Yin, X. Ling, X. Wang, J. Xue, M. Dresselhaus, J. Kong, and B. Yildiz, Tuning electronic structure of single layer MoS_2 through defect and interface engineering, *ACS Nano* 12(3), 2569 (2018)
61. Z. Hu, Y. Zhao, W. Zou, Q. Lu, J. Liao, F. Li, M. Shang, L. Lin, and Z. Liu, Doping of graphene films: Open the way to applications in electronics and optoelectronics, *Adv. Funct. Mater.* 32(42), 2203179 (2022)
62. S. Zhang, C. G. Wang, M. Y. Li, D. Huang, L. J. Li, W. Ji, and S. Wu, Defect structure of localized excitons in a WSe_2 monolayer, *Phys. Rev. Lett.* 119(4), 046101 (2017)
63. R. Yang, J. Fan, and M. Sun, Transition metal dichalcogenides (TMDCs) heterostructures: Optoelectric properties, *Front. Phys.* 17(4), 43202 (2022)
64. M. Tebyetekerwa, Y. Cheng, J. Zhang, W. Li, H. Li, G. P. Neupane, B. Wang, T. N. Truong, C. Xiao, M. M. Al-Jassim, Z. Yin, Y. Lu, D. Macdonald, and H. T. Nguyen, Emission control from transition metal dichalcogenide monolayers by aggregation-induced molecular rotors, *ACS Nano* 14(6), 7444 (2020)
65. J. Kim, Y. Oh, J. Shin, M. Yang, N. Shin, S. Shekhar, and S. Hong, Nanoscale mapping of carrier mobilities in the ballistic transports of carbon nanotube networks, *ACS Nano* 16(12), 21626 (2022)
66. W. Wang, H. Shu, J. Wang, Y. Cheng, P. Liang, and X. Chen, Defect passivation and photoluminescence enhancement of monolayer MoS_2 crystals through sodium halide-assisted chemical vapor deposition growth, *ACS Appl. Mater. Interfaces* 12(8), 9563 (2020)
67. B. Huang, M. Yoon, B. G. Sumpter, S. H. Wei, and F. Liu, Alloy engineering of defect properties in semiconductors: Suppression of deep levels in transition-metal dichalcogenides, *Phys. Rev. Lett.* 115(12), 126806 (2015)
68. M. Yarali, H. Brahmi, Z. Yan, X. Li, L. Xie, S. Chen, S. Kumar, M. Yoon, K. Xiao, and A. Mavrokefalos, Effect of metal doping and vacancies on the thermal conductivity of monolayer molybdenum diselenide, *ACS Appl. Mater. Interfaces* 10(5), 4921 (2018)
69. K. Zhang, B. M. Bersch, J. Joshi, R. Addou, C. R. Cormier, C. Zhang, K. Xu, N. C. Briggs, K. Wang, S. Subramanian, K. Cho, S. Fullerton-Shirey, R. M. Wallace, P. M. Vora, and J. A. Robinson, Tuning the electronic and photonic properties of monolayer MoS_2 via *in situ* rhenium substitutional doping, *Adv. Funct. Mater.* 28(16) (2018)
70. X. Li, A. A. Puretzky, X. Sang, S. Kc, M. Tian, F. Ceballos, M. Mahjouri-Samani, K. Wang, R. R. Unocic, H. Zhao, G. Duscher, V. R. Cooper, C. M. Rouleau, D. B. Geohegan, and K. Xiao, Suppression of defects and deep levels using isoelectronic tungsten substitution in monolayer $MoSe_2$, *Adv. Funct. Mater.* 27(19), 1603850 (2017)
71. W. Chen, J. Zhao, J. Zhang, L. Gu, Z. Yang, X. Li, H. Yu, X. Zhu, R. Yang, D. Shi, X. Lin, J. Guo, X. Bai, and G. Zhang, Oxygen-assisted chemical vapor deposition growth of large single-crystal and high-quality monolayer MoS_2, *J. Am. Chem. Soc.* 137(50), 15632 (2015)
72. Z. Wang, H. Yang, S. Zhang, J. Wang, K. Cao, Y. Lu, W. Hou, S. Guo, X. A. Zhang, and L. Wang, An approach to high-throughput growth of submillimeter transition metal dichalcogenide single crystals, *Nanoscale* 11(46), 22440 (2019)
73. Z. Tu, G. Li, X. Ni, L. Meng, S. Bai, X. Chen, J. Lou, and Y. Qin, Synthesis of large monolayer single crystal MoS_2 nanosheets with uniform size through a double-tube technology, *Appl. Phys. Lett.* 109(22), 223101 (2016)
74. J. Chen, W. Tang, B. Tian, B. Liu, X. Zhao, Y. Liu, T. Ren, W. Liu, D. Geng, H. Y. Jeong, H. S. Shin, W. Zhou, and K. P. Loh, Chemical vapor deposition of high-quality large-sized MoS_2 crystals on silicon dioxide substrates, *Adv. Sci. (Weinh.)* 3(8), 1500033 (2016)
75. H. G. Ji, Y. C. Lin, K. Nagashio, M. Maruyama, P. Solís-Fernández, A. Sukma Aji, V. Panchal, S. Okada, K. Suenaga, and H. Ago, Hydrogen-assisted epitaxial growth of monolayer tungsten disulfide and seamless grain stitching, *Chem. Mater.* 30(2), 403 (2018)
76. Y. Gong, G. Ye, S. Lei, G. Shi, Y. He, J. Lin, X. Zhang, R. Vajtai, S. T. Pantelides, W. Zhou, B. Li, and P. M. Ajayan, Synthesis of millimeter-scale transition metal dichalcogenides single crystals, *Adv. Funct. Mater.* 26(12), 2009 (2016)
77. Z. Lin, Y. Zhao, C. Zhou, R. Zhong, X. Wang, Y. H. Tsang, and Y. Chai, Controllable growth of large-size crystalline mos_2 and resist-free transfer assisted with a Cu thin film, *Sci. Rep.* 5(1), 18596 (2015)
78. S. Wang, M. Pacios, H. Bhaskaran, and J. H. Warner, Substrate control for large area continuous films of monolayer MoS_2 by atmospheric pressure chemical vapor deposition, *Nanotechnology* 27(8), 085604 (2016)
79. P. Yang, X. Zou, Z. Zhang, M. Hong, J. Shi, S. Chen, J. Shu, L. Zhao, S. Jiang, X. Zhou, Y. Huan, C. Xie, P. Gao, Q. Chen, Q. Zhang, Z. Liu, and Y. Zhang, Batch production of 6-inch uniform monolayer molybdenum disulfide catalyzed by sodium in glass, *Nat. Commun.* 9(1), 979 (2018)

80. M. E. Pam, Y. Shi, J. Hu, X. Zhao, J. Dan, X. Gong, S. Huang, D. Geng, S. Pennycook, L. K. Ang, and H. Y. Yang, Effects of precursor pre-treatment on the vapor deposition of WS_2 monolayers, *Nanoscale Adv.* 1(3), 953 (2019)
81. Z. Zhang, X. Xu, J. Song, Q. Gao, S. Li, Q. Hu, X. Li, and Y. Wu, High-performance transistors based on monolayer CVD MoS_2 grown on molten glass, *Appl. Phys. Lett.* 113(20), 202103 (2018)
82. J. Chen, X. Zhao, S. J. R. Tan, H. Xu, B. Wu, B. Liu, D. Fu, W. Fu, D. Geng, Y. Liu, W. Liu, W. Tang, L. Li, W. Zhou, T. C. Sum, and K. P. Loh, Chemical vapor deposition of large-size monolayer $MoSe_2$ crystals on molten glass, *J. Am. Chem. Soc.* 139(3), 1073 (2017)
83. P. Yang, S. Zhang, S. Pan, B. Tang, Y. Liang, X. Zhao, Z. Zhang, J. Shi, Y. Huan, Y. Shi, S. J. Pennycook, Z. Ren, G. Zhang, Q. Chen, X. Zou, Z. Liu, and Y. Zhang, Epitaxial growth of centimeter-scale single-crystal MoS_2 monolayer on Au(111), *ACS Nano* 14(4), 5036 (2020)
84. J. Shi, X. Zhang, D. Ma, J. Zhu, Y. Zhang, Z. Guo, Y. Yao, Q. Ji, X. Song, Y. Zhang, C. Li, Z. Liu, W. Zhu, and Y. Zhang, Substrate facet effect on the growth of monolayer MoS_2 on Au foils, *ACS Nano* 9(4), 4017 (2015)
85. S. J. Yun, S. H. Chae, H. Kim, J. C. Park, J. H. Park, G. H. Han, J. S. Lee, S. M. Kim, H. M. Oh, J. Seok, M. S. Jeong, K. K. Kim, and Y. H. Lee, Synthesis of centimeter-scale monolayer tungsten disulfide film on gold foils, *ACS Nano* 9(5), 5510 (2015)
86. Y. Gao, Z. Liu, D. M. Sun, L. Huang, L. P. Ma, L. C. Yin, T. Ma, Z. Zhang, X. L. Ma, L. M. Peng, H. M. Cheng, and W. Ren, Large-area synthesis of high-quality and uniform monolayer WS_2 on reusable Au foils, *Nat. Commun.* 6(1), 8569 (2015)
87. K. Godin, K. Kang, S. Fu, and E. H. Yang, Increased monolayer domain size and patterned growth of tungsten disulfide through controlling surface energy of substrates, *J. Phys. D Appl. Phys.* 49(32), 325304 (2016)
88. F. Lan, R. Yang, S. Hao, B. Zhou, K. Sun, H. Cheng, S. Zhang, L. Li, and L. Jin, Controllable synthesis of millimeter-size single crystal WS_2, *Appl. Surf. Sci.* 504, 144378 (2020)
89. G. Li, X. Wang, B. Han, W. Zhang, S. Qi, Y. Zhang, J. Qiu, P. Gao, S. Guo, R. Long, Z. Tan, X. Z. Song, and N. Liu, Direct growth of continuous and uniform MoS_2 film on SiO_2/Si substrate catalyzed by sodium sulfate, *J. Phys. Chem. Lett.* 11(4), 1570 (2020)
90. H. Kim, G. H. Han, S. J. Yun, J. Zhao, D. H. Keum, H. Y. Jeong, T. H. Ly, Y. Jin, J. H. Park, B. H. Moon, S. W. Kim, and Y. H. Lee, Role of alkali metal promoter in enhancing lateral growth of monolayer transition metal dichalcogenides, *Nanotechnology* 28(36), 36LT01 (2017)
91. J. G. Song, G. Hee Ryu, Y. Kim, W. Je Woo, K. Yong Ko, Y. Kim, C. Lee, I. K. Oh, J. Park, Z. Lee, and H. Kim, Catalytic chemical vapor deposition of large-area uniform two-dimensional molybdenum disulfide using sodium chloride, *Nanotechnology* 28(46), 465103 (2017)
92. H. Kim, D. Ovchinnikov, D. Deiana, D. Unuchek, and A. Kis, Suppressing nucleation in metal–organic chemical vapor deposition of MoS_2 monolayers by alkali metal halides, *Nano Lett.* 17(8), 5056 (2017)
93. Y. Shi, P. Yang, S. Jiang, Z. Zhang, Y. Huan, C. Xie, M. Hong, J. Shi, and Y. Zhang, Na-assisted fast growth of large single-crystal MoS_2 on sapphire, *Nanotechnology* 30(3), 034002 (2019)
94. B. J. Modtland, E. Navarro-Moratalla, X. Ji, M. Baldo, and J. Kong, Monolayer tungsten disulfide (WS_2) via chlorine-driven chemical vapor transport, *Small* 13(33), 1701232 (2017)
95. P. Yang, A. G. Yang, L. Chen, J. Chen, Y. Zhang, H. Wang, L. Hu, R. J. Zhang, R. Liu, X. P. Qu, Z. J. Qiu, and C. Cong, Influence of seeding promoters on the properties of CVD grown monolayer molybdenum disulfide, *Nano Res.* 12(4), 823 (2019)
96. X. Ling, Y. H. Lee, Y. Lin, W. Fang, L. Yu, M. S. Dresselhaus, and J. Kong, Role of the seeding promoter in MoS_2 growth by chemical vapor deposition, *Nano Lett.* 14(2), 464 (2014)
97. Y. F. Lim, K. Priyadarshi, F. Bussolotti, P. K. Gogoi, X. Cui, M. Yang, J. Pan, S. W. Tong, S. Wang, S. J. Pennycook, K. E. J. Goh, A. T. S. Wee, S. L. Wong, and D. Chi, Modification of vapor phase concentrations in MoS_2 growth using a NiO foam barrier, *ACS Nano* 12(2), 1339 (2018)
98. J. Zhu, H. Xu, G. Zou, W. Zhang, R. Chai, J. Choi, J. Wu, H. Liu, G. Shen, and H. Fan, MoS_2–OH bilayer-mediated growth of inch-sized monolayer MoS_2 on arbitrary substrates, *J. Am. Chem. Soc.* 141(13), 5392 (2019)
99. G. U. Özküçük, C. Odacı, E. Şahin, F. Ay, and N. K. Perkgöz, Glass-assisted CVD growth of large-area MoS_2, WS_2 and $MoSe_2$ monolayers on Si/SiO_2 substrate, *Mater. Sci. Semicond. Process.* 105, 104679 (2020)
100. J. Jiang, Q. Zhang, A. Wang, Y. Zhang, F. Meng, C. Zhang, X. Feng, Y. Feng, L. Gu, H. Liu, and L. Han, A facile and effective method for patching sulfur vacancies of WS_2 via nitrogen plasma treatment, *Small* 15(36), 1901791 (2019)
101. H. Nan, Z. Wang, W. Wang, Z. Liang, Y. Lu, Q. Chen, D. He, P. Tan, F. Miao, X. Wang, J. Wang, and Z. Ni, Strong photoluminescence enhancement of MoS_2 through defect engineering and oxygen bonding, *ACS Nano* 8(6), 5738 (2014)
102. D. Pierucci, H. Henck, Z. Ben Aziza, C. H. Naylor, A. Balan, J. E. Rault, M. G. Silly, Y. J. Dappe, F. Bertran, P. Le Fevre, F. Sirotti, A. T. Johnson, and A. Ouerghi, Tunable doping in hydrogenated single layered molybdenum disulfide, *ACS Nano* 11(2), 1755 (2017)
103. Y. Zhu, H. Yi, Q. Hao, J. Liu, Y. Ke, Z. Wang, D. Fan, and W. Zhang, Scalable synthesis and defect modulation of large monolayer WS_2 via annealing in H_2S atmosphere/thiol treatment to enhance photoluminescence, *Appl. Surf. Sci.* 485, 101 (2019)
104. S. Hu, J. Li, S. Wang, Y. Liang, H. Kang, Y. Zhang, Z. Chen, Y. Sui, G. Yu, S. Peng, Z. Jin, and X. Liu, Detecting the repair of sulfur vacancies in CVD-grown

MoS_2 domains via hydrogen etching, *J. Electron. Mater.* 49(4), 2547 (2020)
105. M. Liu, J. Shi, Y. Li, X. Zhou, D. Ma, Y. Qi, Y. Zhang, and Z. Liu, Temperature-triggered sulfur vacancy evolution in monolayer MoS_2/graphene heterostructures, *Small* 13(40), 1602967 (2017)
106. S. V. Sivaram, A. T. Hanbicki, M. R. Rosenberger, G. G. Jernigan, H. J. Chuang, K. M. McCreary, and B. T. Jonker, Spatially selective enhancement of photoluminescence in MoS_2 by exciton-mediated adsorption and defect passivation, *ACS Appl. Mater. Interfaces* 11(17), 16147 (2019)
107. A. Bera, D. V. S. Muthu, and A. K. Sood, Enhanced Raman and photoluminescence response in monolayer MoS_2 due to laser healing of defects, *J. Raman Spectrosc.* 49(1), 100 (2018)
108. A. Venkatakrishnan, H. Chua, P. Tan, Z. Hu, H. Liu, Y. Liu, A. Carvalho, J. Lu, and C. H. Sow, Microsteganography on WS_2 monolayers tailored by direct laser painting, *ACS Nano* 11(1), 713 (2017)
109. D. Kiriya, Y. Hijikata, J. Pirillo, R. Kitaura, A. Murai, A. Ashida, T. Yoshimura, and N. Fujimura, Systematic study of photoluminescence enhancement in monolayer molybdenum disulfide by acid treatment, *Langmuir* 34(35), 10243 (2018)
110. X. Dai, X. Zhang, I. M. Kislyakov, L. Wang, J. Huang, S. Zhang, N. Dong, and J. Wang, Enhanced two-photon absorption and two-photon luminescence in monolayer MoS_2 and WS_2 by defect repairing, *Opt. Express* 27(10), 13744 (2019)
111. S. Roy, W. Choi, S. Jeon, D. H. Kim, H. Kim, S. J. Yun, Y. Lee, J. Lee, Y. M. Kim, and J. Kim, Atomic observation of filling vacancies in monolayer transition metal sulfides by chemically sourced sulfur atoms, *Nano Lett.* 18(7), 4523 (2018)
112. K. P. Dhakal, S. Roy, S. J. Yun, G. Ghimire, C. Seo, and J. Kim, Heterogeneous modulation of exciton emission in triangular WS_2 monolayers by chemical treatment, *J. Mater. Chem. C Mater. Opt. Electron. Devices* 5(27), 6820 (2017)
113. Y. Kim, Y. Lee, H. Kim, S. Roy, and J. Kim, Near-field exciton imaging of chemically treated MoS_2 monolayers, *Nanoscale* 10(18), 8851 (2018)
114. M. Amani, D. H. Lien, D. Kiriya, J. Xiao, A. Azcatl, J. Noh, S. R. Madhvapathy, R. Addou, S. Kc, M. Dubey, K. Cho, R. M. Wallace, S. C. Lee, J. H. He, J. W. Ager, X. Zhang, E. Yablonovitch, and A. Javey, Near-unity photoluminescence quantum yield in MoS_2, *Science* 350(6264), 1065 (2015)
115. H. Kim, D. H. Lien, M. Amani, J. W. Ager, and A. Javey, Highly stable near-unity photoluminescence yield in monolayer MoS_2 by fluoropolymer encapsulation and superacid treatment, *ACS Nano* 11(5), 5179 (2017)
116. A. Alharbi, P. Zahl, and D. Shahrjerdi, Material and device properties of superacid-treated monolayer molybdenum disulfide, *Appl. Phys. Lett.* 110(3), 033503 (2017)
117. P. Lin, L. Zhu, D. Li, and Z. L. Wang, Defect repair for enhanced piezo-phototronic MoS_2 flexible phototransistors, *J. Mater. Chem. C Mater. Opt. Electron. Devices* 7(46), 14731 (2019)
118. X. Zhang, Q. Liao, S. Liu, Z. Kang, Z. Zhang, J. Du, F. Li, S. Zhang, J. Xiao, B. Liu, Y. Ou, X. Liu, L. Gu, and Y. Zhang, Poly(4-styrenesulfonate)-induced sulfur vacancy self-healing strategy for monolayer MoS_2 homojunction photodiode, *Nat. Commun.* 8(1), 15881 (2017)
119. X. Zhang, Q. Liao, Z. Kang, B. Liu, Y. Ou, J. Du, J. Xiao, L. Gao, H. Shan, Y. Luo, Z. Fang, P. Wang, Z. Sun, Z. Zhang, and Y. Zhang, Self-healing originated van der Waals homojunctions with strong interlayer coupling for high-performance photodiodes, *ACS Nano* 13(3), 3280 (2019)
120. Z. Yu, Y. Pan, Y. Shen, Z. Wang, Z. Y. Ong, T. Xu, R. Xin, L. Pan, B. Wang, L. Sun, J. Wang, G. Zhang, Y. W. Zhang, Y. Shi, and X. Wang, Towards intrinsic charge transport in monolayer molybdenum disulfide by defect and interface engineering, *Nat. Commun.* 5(1), 5290 (2014)
121. L. Zhou, S. Yan, L. Pan, X. Wang, Y. Wang, and Y. Shi, A scalable sulfuration of WS_2 to improve cyclability and capability of lithium-ion batteries, *Nano Res.* 9(3), 857 (2016)
122. S. Bertolazzi, S. Bonacchi, G. Nan, A. Pershin, D. Beljonne, and P. Samori, Engineering chemically active defects in monolayer MoS_2 transistors via ion-beam irradiation and their healing via vapor deposition of alkanethiols, *Adv. Mater.* 29(18), 1606760 (2017)
123. M. Makarova, Y. Okawa, and M. Aono, Selective adsorption of thiol molecules at sulfur vacancies on MoS_2(0001), followed by vacancy repair via S–C dissociation, *J. Phys. Chem. C* 116(42), 22411 (2012)
124. M. El Garah, S. Bertolazzi, S. Ippolito, M. Eredia, I. Janica, G. Melinte, O. Ersen, G. Marletta, A. Ciesielski, and P. Samorì, MoS_2 nanosheets via electrochemical lithium-ion intercalation under ambient conditions, *FlatChem* 9, 33 (2018)
125. K. Cho, M. Min, T. Y. Kim, H. Jeong, J. Pak, J. K. Kim, J. Jang, S. J. Yun, Y. H. Lee, W. K. Hong, and T. Lee, Electrical and optical characterization of MoS_2 with sulfur vacancy passivation by treatment with alkanethiol molecules, *ACS Nano* 9(8), 8044 (2015)
126. Q. Ding, K. J. Czech, Y. Zhao, J. Zhai, R. J. Hamers, J. C. Wright, and S. Jin, Basal-plane ligand functionalization on semiconducting 2H-MoS_2 monolayers, *ACS Appl. Mater. Interfaces* 9(14), 12734 (2017)
127. D. M. Sim, M. Kim, S. Yim, M. J. Choi, J. Choi, S. Yoo, and Y. S. Jung, Controlled doping of vacancy-containing few-layer MoS_2 via highly stable thiol-based molecular chemisorption, *ACS Nano* 9(12), 12115 (2015)
128. S. Wei, C. Ge, L. Zhou, S. Zhang, M. Dai, F. Gao, Y. Sun, Y. Qiu, Z. Wang, J. Zhang, and P. Hu, Performance improvement of multilayered SnS_2 field effect transistors through synergistic effect of vacancy repairing and electron doping introduced by EDTA, *ACS Appl. Electron. Mater.* 1(11), 2380 (2019)
129. J. H. Park, A. Sanne, Y. Guo, M. Amani, K. Zhang, H. C. P. Movva, J. A. Robinson, A. Javey, J. Robertson, S. K. Banerjee, and A. C. Kummel, Defect passivation of transition metal dichalcogenides via a charge transfer

van der Waals interface, *Sci. Adv.* 3(10), e1701661 (2017)

130. W. Ding, X. Li, F. Jiang, P. Liu, P. Liu, S. Zhu, G. Zhang, C. Liu, and J. Xu, Defect modification engineering on a laminar MoS_2 film for optimizing thermoelectric properties, *J. Mater. Chem. C* 8(6), 1909 (2020)
131. A. O. A. Tanoh, J. Alexander-Webber, J. Xiao, G. Delport, C. A. Williams, H. Bretscher, N. Gauriot, J. Allardice, R. Pandya, Y. Fan, Z. Li, S. Vignolini, S. D. Stranks, S. Hofmann, and A. Rao, Enhancing photoluminescence and mobilities in WS_2 monolayers with oleic acid ligands, *Nano Lett.* 19(9), 6299 (2019)
132. D. H. Luong, H. S. Lee, G. Ghimire, J. Lee, H. Kim, S. J. Yun, G. H. An, and Y. H. Lee, Enhanced light–matter interactions in self-assembled plasmonic nanoparticles on 2D semiconductors, *Small* 14(47), 1802949 (2018)
133. T. L. Atallah, J. Wang, M. Bosch, D. Seo, R. A. Burke, O. Moneer, J. Zhu, M. Theibault, L. E. Brus, J. Hone, and X. Y. Zhu, Electrostatic screening of charged defects in monolayer MoS_2, *J. Phys. Chem. Lett.* 8(10), 2148 (2017)
134. J. Jiang, C. Ling, T. Xu, W. Wang, X. Niu, A. Zafar, Z. Yan, X. Wang, Y. You, L. Sun, J. Lu, J. Wang, and Z. Ni, Defect engineering for modulating the trap states in 2D photoconductors, *Adv. Mater.* 30(40), e1804332 (2018)
135. X. Xu, Z. Chen, B. Sun, Y. Zhao, L. Tao, and J. B. Xu, Efficient passivation of monolayer MoS_2 by epitaxially grown 2D organic crystals, *Sci. Bull. (Beijing)* 64(22), 1700 (2019)
136. S. Mouri, Y. Miyauchi, and K. Matsuda, Tunable photoluminescence of monolayer MoS_2 via chemical doping, *Nano Lett.* 13(12), 5944 (2013)
137. L. Yang, K. Majumdar, H. Liu, Y. Du, H. Wu, M. Hatzistergos, P. Y. Hung, R. Tieckelmann, W. Tsai, C. Hobbs, and P. D. Ye, Chloride molecular doping technique on 2D materials: WS_2 and MoS_2, *Nano Lett.* 14(11), 6275 (2014)
138. J. Lu, A. Carvalho, X. K. Chan, H. Liu, B. Liu, E. S. Tok, K. P. Loh, A. H. Castro Neto, and C. H. Sow, Atomic healing of defects in transition metal dichalcogenides, *Nano Lett.* 15(5), 3524 (2015)
139. L. Wang, M. Schmid, Z. N. Nilsson, M. Tahir, H. Chen, and J. B. Sambur, Laser annealing improves the photoelectrochemical activity of ultrathin $MoSe_2$ photoelectrodes, *ACS Appl. Mater. Interfaces* 11(21), 19207 (2019)
140. H. V. Han, A. Y. Lu, L. S. Lu, J. K. Huang, H. Li, C. L. Hsu, Y. C. Lin, M. H. Chiu, K. Suenaga, C. W. Chu, H. C. Kuo, W. H. Chang, L. J. Li, and Y. Shi, Photoluminescence enhancement and structure repairing of monolayer $MoSe_2$ by hydrohalic acid treatment, *ACS Nano* 10(1), 1454 (2016)
141. Y. Meng, C. Ling, R. Xin, P. Wang, Y. Song, H. Bu, S. Gao, X. Wang, F. Song, J. Wang, X. Wang, B. Wang, and G. Wang, Repairing atomic vacancies in single-layer $MoSe_2$ field-effect transistor and its defect dynamics, *npj Quant. Mater.* 2(1), 16 (2017)
142. H. Ahn, Y. C. Huang, C. W. Lin, Y. L. Chiu, E. C. Lin, Y. Y. Lai, and Y. H. Lee, Efficient defect healing of transition metal dichalcogenides by metallophthalocyanine, *ACS Appl. Mater. Interfaces* 10(34), 29145 (2018)
143. Y. Li, M. Yang, Y. Lu, D. Cao, X. Chen, and H. Shu, Reversible doping polarity and ultrahigh carrier density in two-dimensional van der Waals ferroelectric heterostructures, *Front. Phys.* 18(3), 33307 (2023)